HOCHSCHULE ZITTAU/GÖRLITZ

(FH) - University of Applied Sciences

Ref.: HZG-IPM 610334/3/2.03/F

DELIVERY D27 (Work package 3)

Task 3.1 Experimental Validation

Authorised administrative official:

Dr.-Ing. P. Reinhold
(Chancellor)

Signature

Authorised contact person:

Prof. Dr.-Ing. F. Worlitz
(Project Leader)

Signature

Zittau, 09/30/2005

EUROPEAN COMMISSION
5th EURATOME FRAMEWORK PROGRAMME 1998-2002
KEY ACTION: NUCLEAR FISSION

HTR-E

High-Temperature Reactor Components and Systems

Contract N°
FIKI-CT-2001-00177

Delivery D 27 – Work package 3
3.1 Experimental Validation

Martin Gronek
Steffen Gärtner

University of Applied Sciences Zittau/Görlitz

GERMANY

Dissemination level: RE
Document N°: HTR-E-05/09-D-3-3-1-1
Status: Final
Delivery N°: D27

Modifications

Revision	*Date*	*Modifications*
A	09/30/2005	First Issue

Summary

The document contributes to the 5th Framework Programme HTR-E Work package 3, Delivery D27 – Experimental Validation. It describes the results of the experiments which were performed to determine the static and dynamic limits of the Active Magnetic Bearings (AMB's) and to validate the diagnostic algorithms for magnetic suspended turbo machines.
The experiments were performed under downscaled conditions regarding the functional requirements of the GT-MHR for the following operational and disturbance conditions:

- speed levels and unbalances
- static loads
- dynamic loads

The results of the experiments were compared with the calculated results from simulation to validate the simulation tool MLDyn.

List of Symbols

α	bearing specific constant
γ	rotation angle
$\Delta\varphi$	phase difference
ω	radian frequency
ζ	ratio of disturbance to undisturbed amplitude of rotor displacement
DT	rotating circle diameter of a roller bearing
DW	diameter of a roller bearing
e	eccentricity
f_C	bearing cage rotation frequency
f_n	relative rotation between inner and outer ring of a roller bearing
f_I	roll over frequency
f_O	roll over frequency of the outer bearing ring of a roller bearing
f_R	rolling elements rotation frequency of a roller bearing
Frbb	radial force between the upper and lower bearing level
Frlb	radial force in the level of the lower bearing
Frob	radial force below the lower or over the upper bearing level
Frub	radial force in the level of the upper bearing
h(t)	scaled transition function
i	current
i_-	negative coil current
i_+	positive coil current
$\overline{q}$	mean value
$\tilde{q}$	root mean square (rms)
$r\,q$	vector magnitude
s	rotor displacement
t	time
T	time constant
t_c	compensation time
T_c	time constant for disturbance compensation
Ubb	unbalance between the upper and lower bearing level
Ulb	unbalance in the lower bearing level
Uob	unbalance below the lower or over the upper bearing level
Uub	unbalance in the upper bearing level
Uw	unbalance warp
z	number of rolling elements

Indexes

l	lower level
max	maxima
n	counting index
rad	radial
u	upper level
unb	unbalance
x,y,z	in x-, y-, z-direction

Content

1 Introduction/Objectives

2 Description of FLP500 test facility

3 Mechanical loads
3.1 General test conditions
3.2 Results of the performed experiments
3.2.1 Speed levels and unbalances
3.2.2 Static loads
3.2.3 Dynamic loads
3.3 Comparison experiment with simulation
3.4 Conclusions

4 Validation of diagnostic algorithms
4.1 Introduction
4.2 Results of the performed experiments
4.2.1 Reference values and speed dependence of the features
4.2.2 Identification of internal and external loads
4.3 Validation of the diagnostic models
4.3.1 “Radial force”
4.3.2 “Unbalances”
4.4 Monitoring of limit values and gradients
4.5 Conclusions

1 Introduction/Objectives

The document contributes to the 5th Framework Programme HTR-E Work package 3, Delivery D27 – Experimental Validation. It describes the results of the experiments, which were performed on the AMB test facility FLP500 in Zittau, Germany.

The objective of this task is to determine the static and dynamic limits of the AMB's with scaled boundary conditions of the HTR turbo machine. Therefore the experiments were done under the following conditions:

- speed levels and unbalances
- static loads
- dynamic loads

The experiments for static and dynamic loads were once performed without revolving rotor and once with an rotational speed of 1500 rpm.
The simulation tool MLDyn has to be validated by comparing the simulation results with the measured results from the experiments.

The used inputs are based on the functional requirements for the HTR turbo machine, given in the following document:

Mechanical loads at the turbo machine
Document: HTR-E – AMB and CB – Functional Requirements
HTR-E-02/06-D-3-1-1

Document: HTR-E – Load Analysis – Real Time Investigations
HTR-E-03/10-D-3-1-2-2

2 Description of FLP500 test facility

The FLP500 test facility consists of an vertical arranged rotor shaft with upper and lower radial AMB's and an axial AMB, as shown in Fig. 2.1. Both radial AMB's have a redundant arrangement, that is moved 45 degrees to the main axis's and is acting in the same level (Fig. 2.2)
A magnetic load device is mounted on the lower end of the test facility. The load capacity of the FLP500 is given in Table 3.1.
Further values are:

- nominal air gap of the radial AMB's: 1 mm,
- rotor mass: 1500 kg.

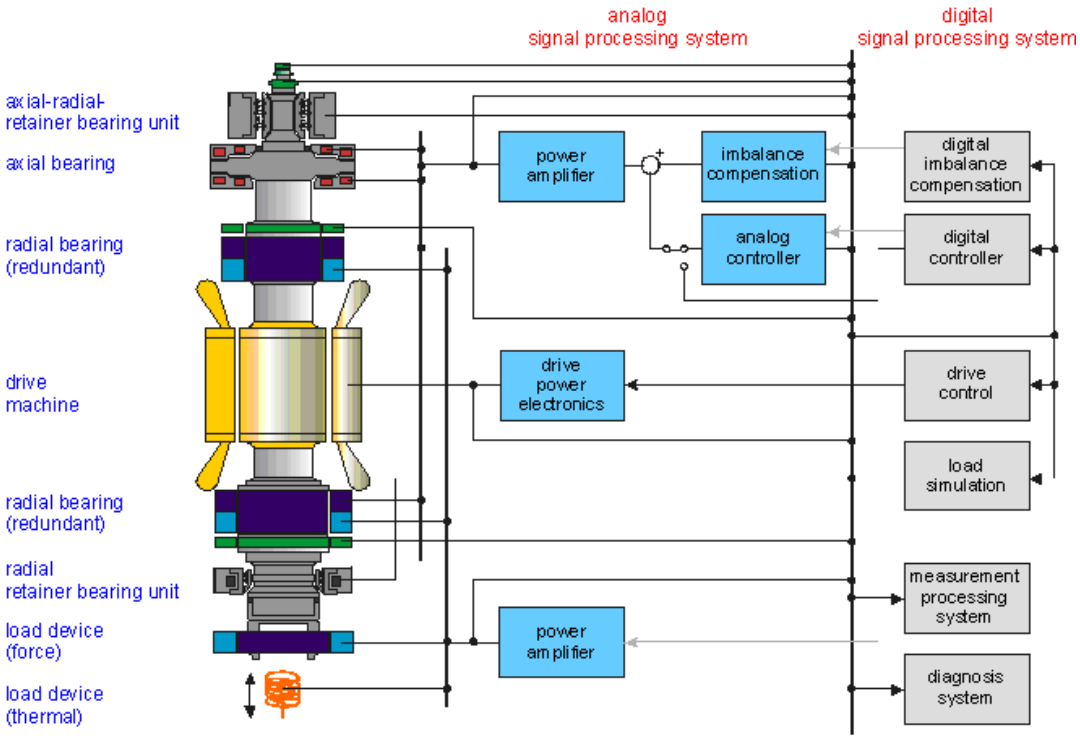

Fig. 2.1: Scheme of the test facility FLP500

The redundant AMB's and the magnetic load device are used to simulate disturbances on the rotor on the different levels as shown in the scheme in Fig. 2.2 for the radial AMB's. While the rotor position is measured in x- and y-direction with position sensors, the load is introduced 45° moved to the main axises. The load introduction in the magnetic load device is is acting in y-direction.

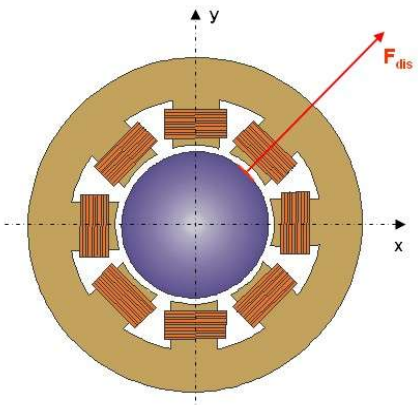

Fig. 2.2: Scheme of radial AMB using redundant AMB for load introduction

Determining the controller performance

For the time constant determination the step response of an static load of 850 N was measured for the upper and lower radial AMB's in y-direction (Fig. 2.3). The conditions are valid from the maximum rotor displacement until reaching the tolerance band of plus/minus 3 Micrometers which represents the signal noise of the position sensors. The time delay for disturbance compensation is as follows:

Upper radial AMB: t_c = 220 sec
Lower radial AMB: t_c = 160 sec

The time constants of disturbance compensation can be determined in a broadly approximation with the 63%-Method which is valid for the transition function of a 1st order delay line member, under the assumption that time constants of higher order, compared with T_c, are very small :

$$h(t)=1-e^{-\frac{t}{T}} \quad \text{for t = T} \quad h(t=T)=1-e^{-\frac{T}{T}}=1-e^{-1}=0{,}63 \tag{2.1}$$

where h(t) is the scaled transition function.

Using this method for approximation the step response the equation changes to:

$$h(t)=1-(1-e^{-\frac{t}{T}})=e^{-\frac{t}{T}} \qquad h(t=T)=e^{-\frac{T}{T}}=e^{-1}=0{,}37 \tag{2.2}$$

Upper radial AMB: T_c = 37,5 sec
Lower radial AMB: T_c = 42,2 sec

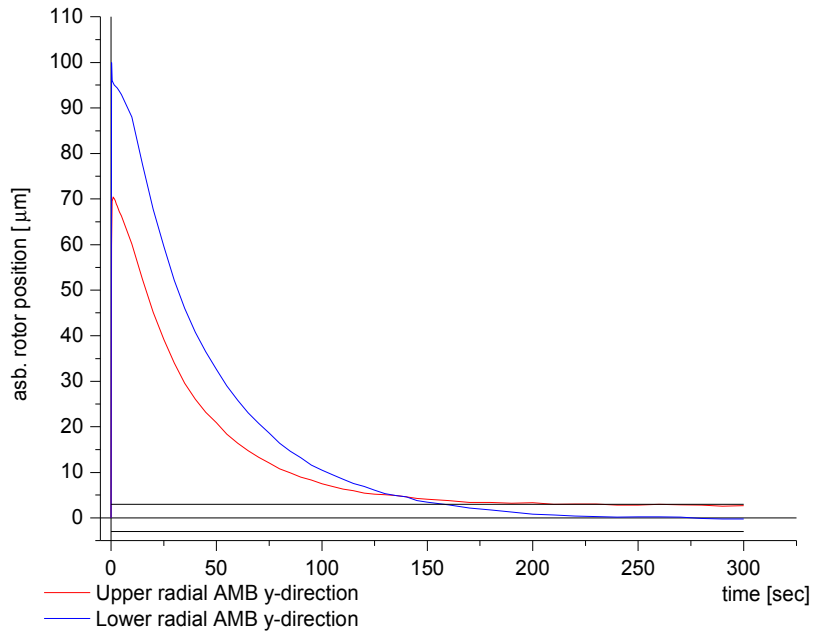

Fig. 2.3: Step response: absolute rotor position vs. time

3 Mechanical loads

3.1 General test conditions

The load capacity of the FLP500 is the following:

Table 3.1: Load capacity FLP500

Unit	***Force***
Upper radial AMB	0.6×10^4 N
Upper redundant radial AMB	0.6×10^4 N
Lower radial AMB	1.0×10^4 N
Lower redundant radial AMB	1.0×10^4 N
Magnetic load device	1.0×10^4 N

The load capacity of the GT-MHR is given in Table 3.2.

Table 3.2: Load capacity GT-MHR

Unit	***Force***
radial AMB 1	6.0×10^4 N
radial AMB 2	12.0×10^4 N
radial AMB 3	12.0×10^4 N
radial AMB 4	6.0×10^4 N
radial AMB 5	6.0×10^4 N
radial AMB 6	6.0×10^4 N

Therefore the following downscaling conditions were used for the experiments:
- radial forces: downscaled 10:1 regarding the load capacity of the radial bearings GT-MHR:FLP500
- frequencies: original

Working with test rigs under downscaling conditions is a usual method described by OKBM [1].

The investigations are based on the following requirements of the GT-MHR [2]:
- radial electromagnetic forces caused by eccentricity of the rotor in the generator stator (acting only on radial bearings N° 2 and N° 3) **0.85×10^4 N**
- resonance frequencies range **0-60 Hz**

Regarding the downscaling conditions and the requirements of the GT-MHR, the experiments, excepted speed levels, were performed with a load of **0.85×10^3 N**.

The evaluation of measurement was done for the most affected AMB's. The following table gives an overview:

Table 3.3: Overview of evaluated parameters

Position of load introduction	***Most affected AMB***
Upper radial redundant AMB	Upper radial AMB x- and y-direction
Lower radial redundant AMB	Lower radial AMB x- and y-direction
Load device	Upper radial AMB y-direction, Lower radial AMB y-direction

3.2 Results of the performed experiments

3.2.1 Speed levels and unbalances

These experiments were once performed for controlled acceleration with different acceleration values and once for single speed levels up to 1500 rpm in a step size of 100 rpm. The objective of these experiments was to determine the influence of unbalances due to the rotational speed.

Controlled acceleration:

For the controlled acceleration the following test conditions obtain:

Table 3.4: Test conditions for controlled acceleration

N°	***Speed range***	***Acceleration***
1	0 up to 1500 rpm	10 rpm/s
2	0 up to 1500 rpm	20 rpm/s
3	0 up to 1500 rpm	30 rpm/s

The position of the revolving rotor is influenced by vibrations, which are caused by unbalances. The reason for these is the eccentricity of the centre of gravity and a problem of tolerances in the manufacturing of the rotor shaft. Unbalances mean loads at the shaft that are rising with the rotational speed. Critical conditions occur for resonance frequencies.
Fig. 3.1 shows exemplary for the upper radial AMB's the amplitude of rotor displacement vs. the rotational speed with three different accelerations. As can be seen, the acceleration has not much influence on the rotor displacement. Over the tested speed range the rotor displacement does not exceed a value of 100 µm, which is ten percent of the nominal air gap.

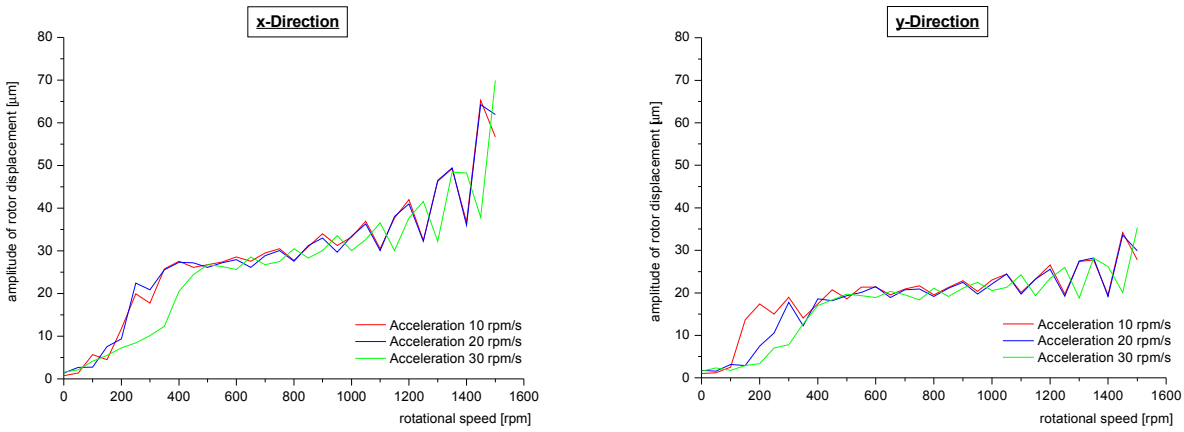

Fig. 3.1: Amplitude of rotor displacement vs. Rotational speed for upper radial AMB's in x- and y-direction

Note: The amplitude of rotor displacement for the lower AMB's can be seen in Annex 1.

Single speed levels:

For this experiment the following test conditions obtain:

- Speed range: 100 up to 1500 rpm
- step size for speed levels: 100 rpm

For each speed level the amplitude of rotor displacement was determined after reaching the steady state vibrations. The speed level of 1000 rpm couldn't be driven, while there occur to strong vibrations in the direction of the axial bearing, as can be seen in Fig. 3.2. This does not matter when this rotational speed is driven through fast enough (compare controlled acceleration)

Fig. 3.2 shows the amplitude of rotor displacement for all AMB's.

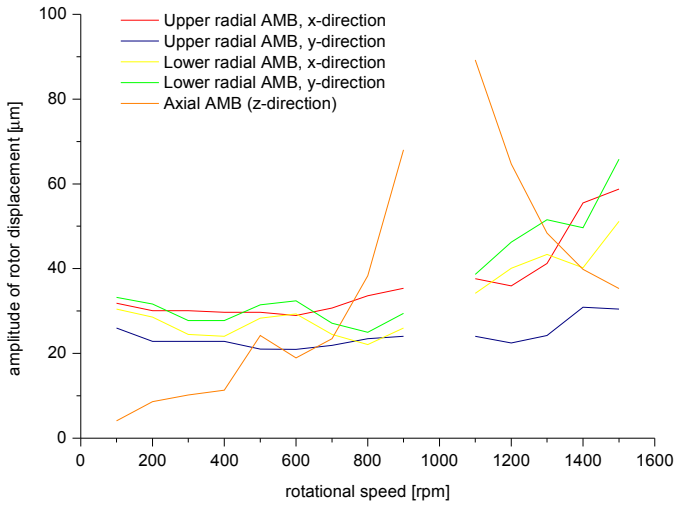

Fig. 3.2: Amplitude of rotor displacement vs. rotational speed

For the tested speed levels the amplitude of rotor displacement for the radial AMB's does not exceed a value of 100 µm.

Fig. 3.3 shows the orbit plane in the level of the lower AMB's for the rotational speed of 1500 rpm. The orbit radius is equal to the amplitude in each direction of the AMB's and there are only small variations around the median orbit.

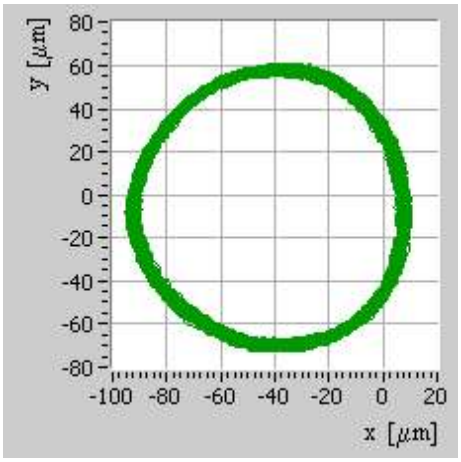

Fig. 3.3: Orbit plane in the level of the lower AMB's on 1500 rpm

3.2.2 Static loads

The objective of these experiments was to determine the influence of a static load as given in the functional requirements for the GT-MHR, acting between the Bearings N° 2 and N° 3. The experiments were once performed without revolving rotor and once with a rotational speed of 1500 rpm. The load was introduced as a step function and as a ramp in each level of the radial AMB's and in the level of the load device (compare with Description of FLP500 test facility).

<u>Step-function:</u>

For the load introduction via step function the following test conditions obtain:
- value of load: 850 N
- duration time of load introduction: 50 sec

Fig. 3.4 shows the load introduction function.

Fig. 3.4: disturbance vs. time

Step-function at 0 rpm:

Fig. 3.5 shows exemplary the step-function response for the load introduction in the level of the upper radial AMB at the non revolving rotor.

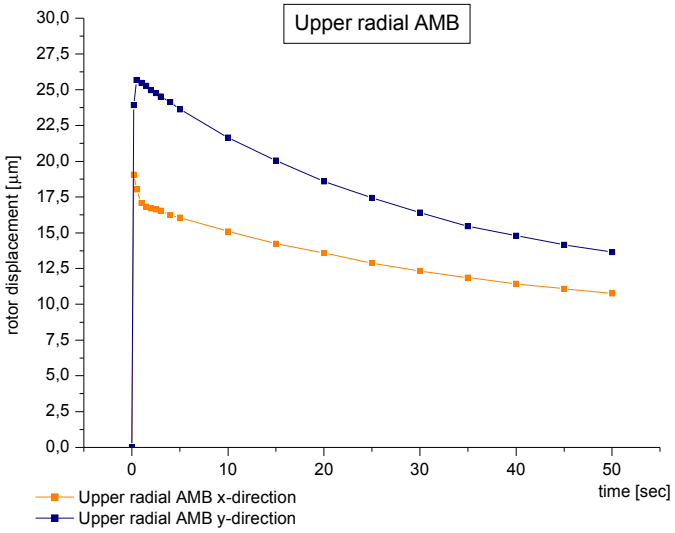

Fig. 3.5: Step-function response in the upper radial AMB

The maximum displacement in each direction was determined from the measurement as follows:
x-direction: 35,45 µm
y-direction: 32,17 µm

Depending on the controller parameters and the load capacity of the AMB, the disturbance compensation effectuates the slowly decreasing of the rotor displacement (compare description of FLP500 test facility).

Step-function at 1500 rpm:

Fig. 3.6 shows exemplary the step-function response for the load introduction in the level of the upper radial AMB at a rotational speed of 1500 rpm.

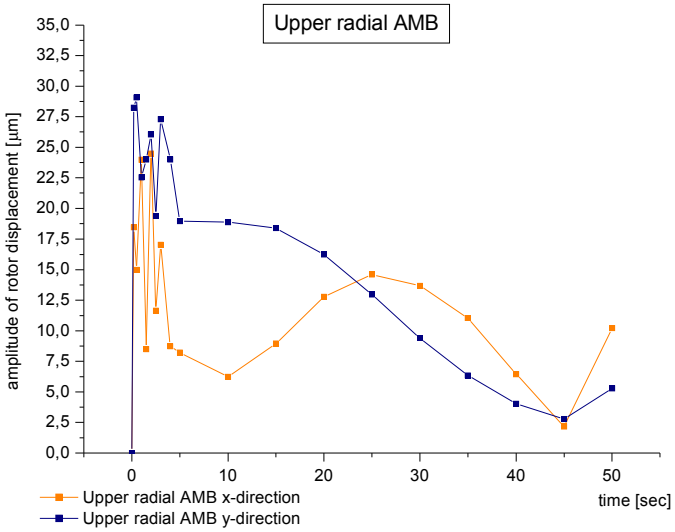

Fig. 3.6: Step-function response in the upper radial AMB

The maximum displacement in each direction was determined from the measurement as follows:
x-direction: 56,32 µm
y-direction: 59,49 µm

The maximum rotor displacement does not exceed a value of 100 µm. The step-function response is overlaid by the vibrations of the rotor, which were caused by unbalances.

Note: For the experiments without revolving rotor and with a rotational speed of 1500 rpm, the step-function response for the load introduction in the levels of the lower AMB's and the load device can be seen in Annex 2.

Ramp:

For the load introduction via ramp the following test conditions obtain:
- maximum value of load: 850 N
- rise time: 30 sec
- duration time on maximum load: 10 sec
- drop-out time: 20 sec

Fig. 3.7 shows the load introduction function.

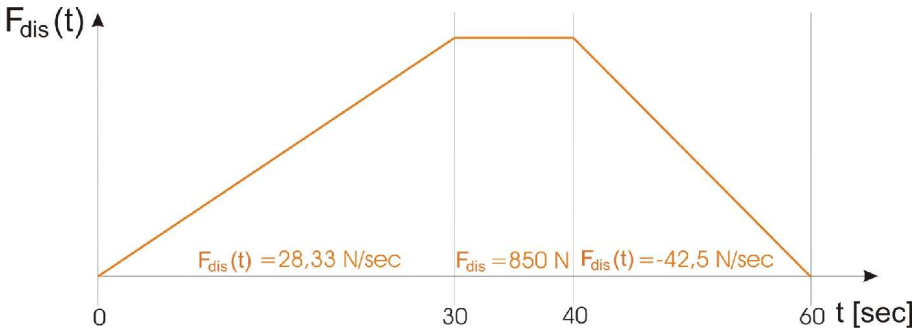

Fig. 3.7: disturbance vs. time

Ramp at 0 rpm:

Fig. 3.8 shows exemplary the ramp response for the load introduction in the level of the upper radial AMB on the non revolving rotor.

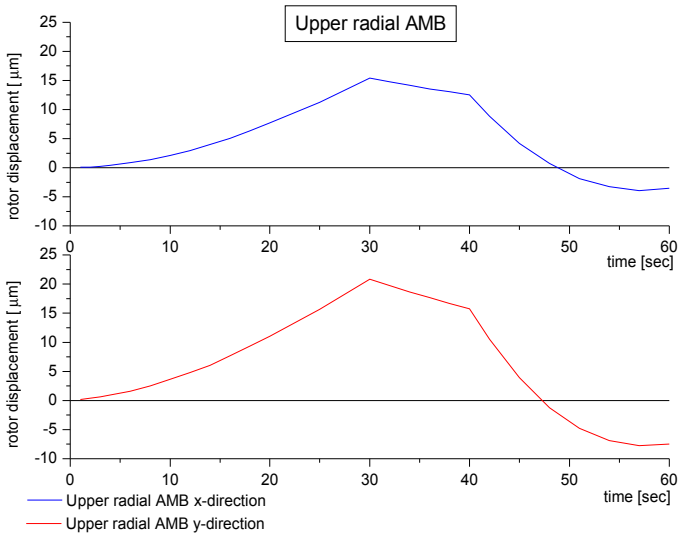

Fig. 3.8: Ramp response in the upper radial AMB

Comparing the disturbance with the systems response (Fig. 3.7 and Fig. 3.8), the rotor displacement increases with the rising of the load. While the load is constant at its maximum value, the rotor displacement decreases slowly as known from the experiments with the step-function disturbance. In the drop-out range, the disturbance compensation of the controller and the load decreasing are acting in the same direction. Therefore the rotor displacement reaches an overshoot in the opposite direction.

Based on the maximum force values, determined from the measurement, the value of the maximum rotor displacement is about 28 µm.

Ramp at 1500 rpm:

Fig. 3.9 shows exemplary the ramp response for the load introduction in the level of the upper radial AMB at a rotational speed of 1500 rpm.

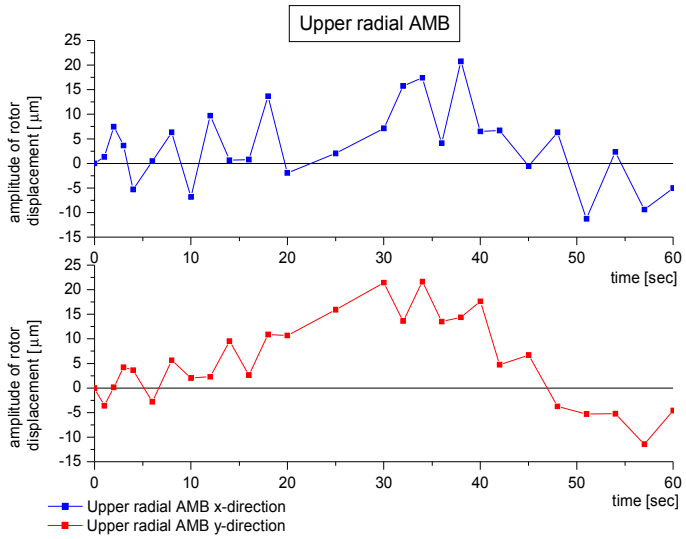

Fig. 3.9: Ramp response in the upper radial AMB

The ramp response is similar to the experiment with the non revolving rotor. As can be seen in Fig. 3.9 there are oscillations (caused by the influence of the vibrations) overlaid while the response has tendentiously the same regime.

The results of the experiments on static loads show a good accordance to the results of the real time investigations, given in the task 1.2 Load Analysis (Delivery D22).
The maximum rotor displacement has the same magnitude as determined by simulation (comp. [3], Annex 2).

Note: For the experiments without revolving rotor and with a rotational speed of 1500 rpm, the ramp response for the load introduction in the levels of the lower AMB's and the load device can be seen in Annex 2.

3.2.3 Dynamic loads

The objective of these experiments was to determine the influence of an oscillating load for the frequency range up to 60 Hz, as given in the functional requirements for the GT-MHR. The experiments were once performed without revolving rotor and once with a rotational speed of 1500 rpm. The load was introduced as a sinusoidal function in each level of the radial AMB's and in the level of the load device.
Additional there was tested the influence of different controller gains by modify them in each direction of the upper radial AMB's.

For the load introduction the following conditions obtain:
- step width of frequency: 5 Hz
- tested frequency range: 5 to 60 Hz
- static offset: 425 N
- Amplitude of oscillating load: 425 N

Fig. 3.10 shows qualitative the load introduction function.

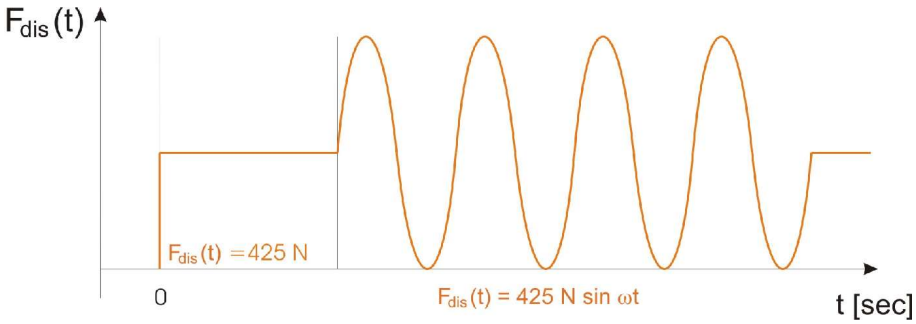

Fig. 3.10: sinusoidal disturbance vs. Time

The criteria for these experiments is the ratio of disturbance to undisturbed amplitude of rotor displacement. Therefore the symbol ζ should be used:

$$\zeta = \frac{amplitude\ of\ rotor\ displacement\ caused\ by\ disturbance\ force}{amplitude\ of\ natural\ rotor\ displacement} \tag{3.1}$$

Sinusoidal at 0 rpm:

Fig. 3.11 shows exemplary the ratio of disturbance to undisturbed amplitude of rotor displacement versus the frequency of the sinusoidal load for the load introduction in the level of the upper radial AMB on the non revolving rotor.

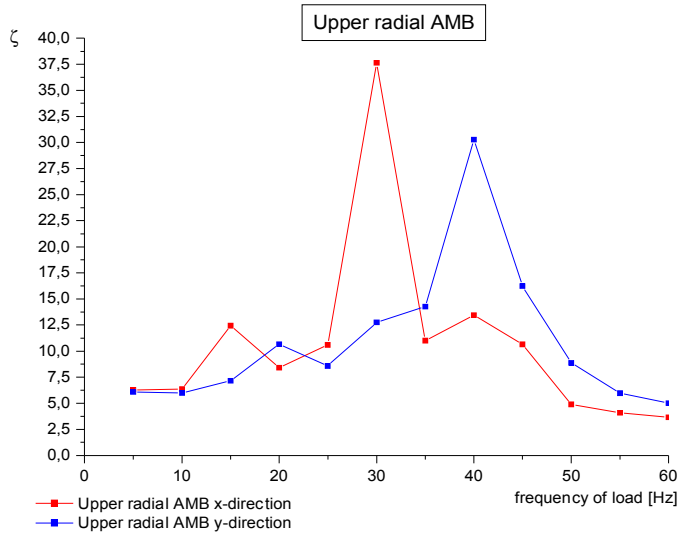

Fig. 3.11: ratio of disturbance to undisturbed amplitude of rotor displacement vs. frequency of load for the upper radial AMB

For the upper radial AMB, the rotor displacement reaches a critical stage in the range between 30 and 40 Hz. The reason is a resonance of the frequency of load and the eigenfrequency of the magnetic suspended system. Caused by the different controller gain in x- and y-direction, the resonances occur at different frequencies. Consequently the influence of the controller gain for the eigenfrequency of the magnetic suspended system is demonstrated.
The maximum rotor displacement was about 80 µm wherefore the damping of the system is sufficient

For higher frequencies the influence of the disturbance decreases after crossing the limit value of the dynamic stiffness.

Sinusoidal at 1500 rpm:

Fig. 3.12 shows exemplary the ratio of disturbance to undisturbed amplitude of rotor displacement versus the frequency of the sinusoidal load for the load introduction in the level of the upper radial AMB at a rotational speed of 1500 rpm.

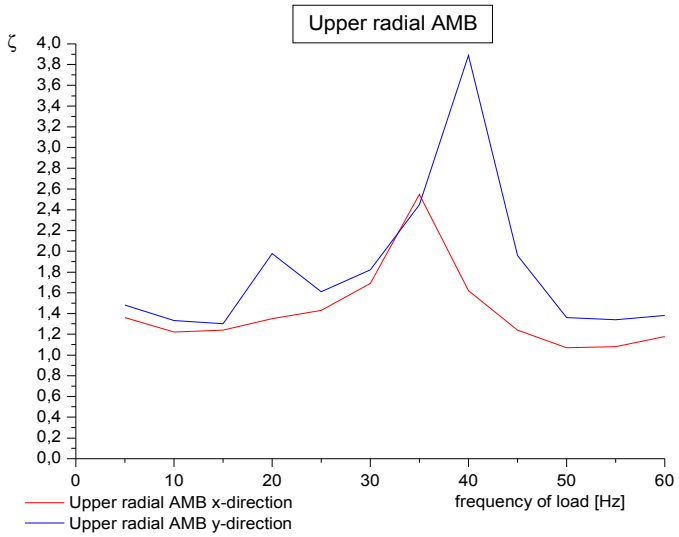

Fig. 3.12: ratio of disturbance to undisturbed amplitude of rotor displacement vs. frequency of load for the upper radial AMB

At a rotational speed of 1500 rpm the ratio of disturbed to undisturbed rotor displacement is about 10 times smaller then at the non revolving rotor. This is because the vibrations of the rotor are overlaid and the influence of the dynamic load decreases.

The results of the experiments on dynamic loads show a good accordance to the results of the real time investigations. Fig. 3.13 shows exemplary the characteristics diagram which was determined for the radial AMB N° 2 of the GT-MHR turbo machine [3]

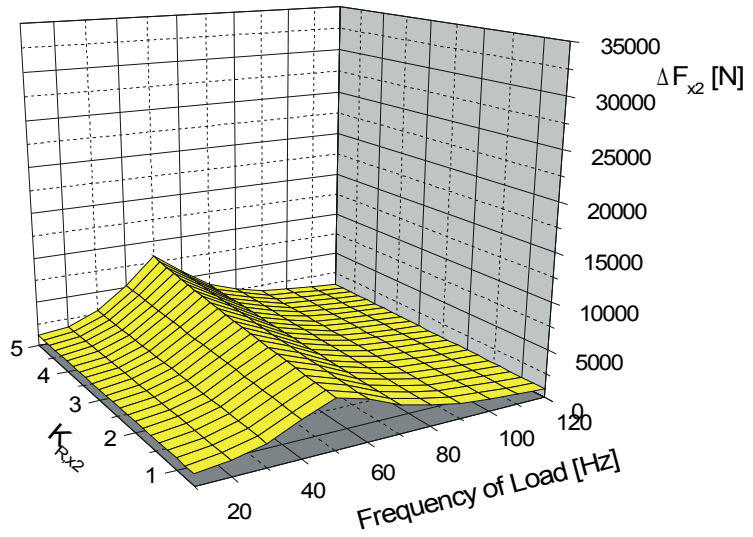

Fig. 3.13: Bearing Force vs. Frequency of Load and Controller Gain

The bearing force is proportional to the rotor displacement. As can be seen in Fig. 3.13 together with Figures 3.11 and 3.12, the highest bearing force occur in the same range of frequency as the maximum rotor displacement, determined by experiment.

Note: For the experiments without revolving rotor and with a rotational speed of 1500 rpm, the response of sinusoidal disturbance for the load introduction in the levels of the lower AMB's and the load device can be seen in Annex 3.

3.3 Comparison experiment with simulation

The objective of this subsection is to validate the simulation tool MLDyn by comparing the measured values from experiment with the results of the simulation. Therefore the simulation tool was parametrized with the test conditions of the experiments, performed at the FLP500 test facility.

The Figures hereafter shows exemplary the good accordance between experiment and simulation. The conditions for this example are as follows:

- Load: 850 N
- Disturbance function: step and sinusoidal with 35 Hz
- Acting in the level of the Load device
- Rotational speed: non

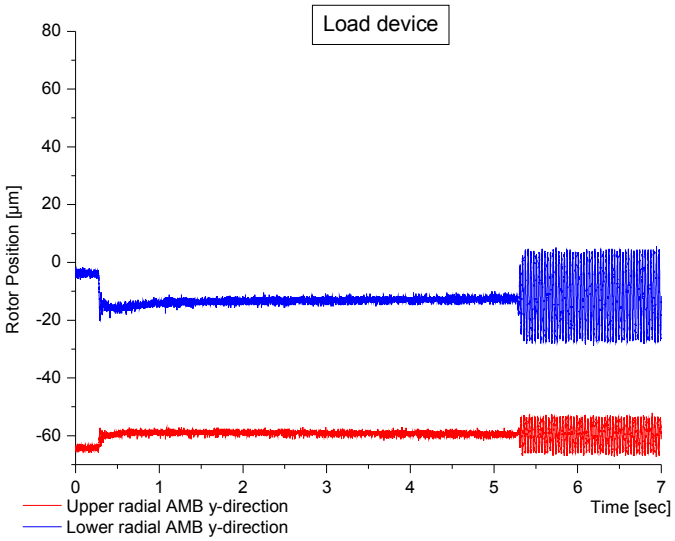

Fig. 3.14: Measurement from experiment: Rotor position vs. time

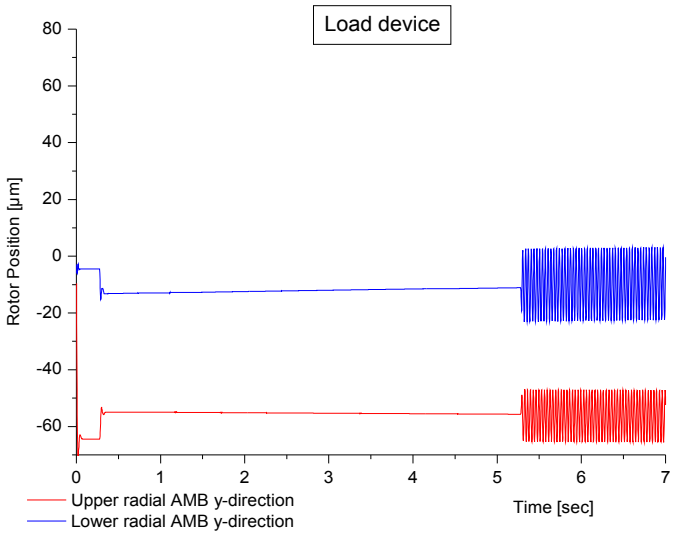

Fig. 3.15: Results from simulation: Rotor position vs. time

Fig. 3.16 and Fig. 3.17 shows in detail the change from step response to the response of the sinusoidal disturbance.

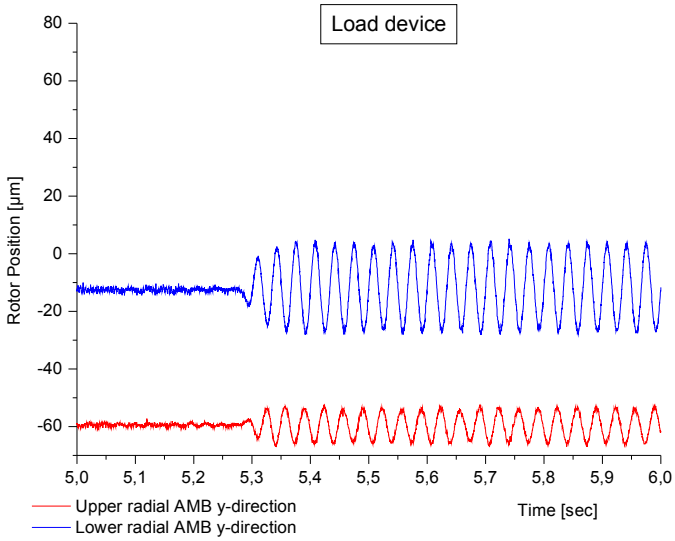

Fig. 3.16: Measurement from experiment in detail: Rotor position vs. time

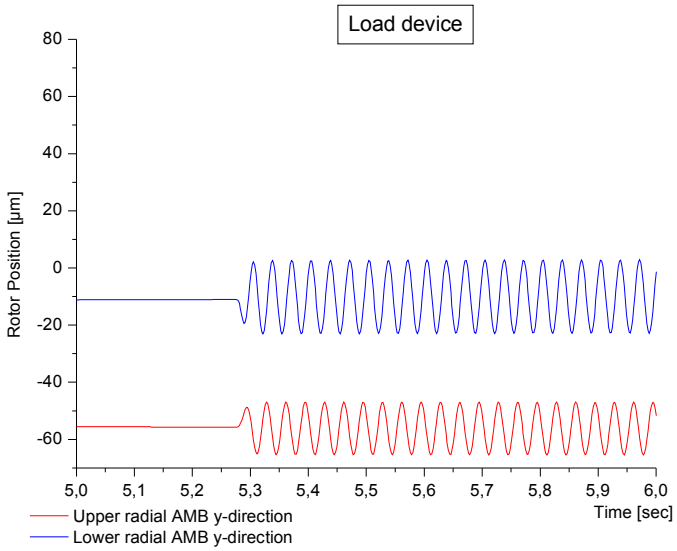

Fig. 3.17: Results from simulation in detail: Rotor position vs. time

The amplitude of rotor displacement in experiment and simulation has the same magnitude, as can be seen in Figures 3.16 and 3.17. The only difference is a signal noise from the position sensor, which is overlaid in the values from the measurement.

This example proves the applicability of the simulation tool MLDyn for the determination of the behaviour of magnetic suspended turbo machines. So MLDyn is a basis for investigations of the behaviour of magnetic bearings.

The experiments under downscaled conditions prove that:
- the AMB's are applicable for the frequency range of loads
- the necessary dynamic stiffness is given by the AMB's

3.4 Conclusions

Regarding the task “Experimental Validation“ experiments were performed at the FLP500 test facility to determine the static and dynamic limits of the AMB's. The results from the experiments show a good accordance to the results of the Real Time Investigations which were performed in the task ”1.2 Load Analysis“.
The experiments were performed under the following operational and disturbances conditions:

- speed levels and unbalances
- static loads
- dynamic loads

Results:

Investigation	***Parameters***	***Criteria***	***Results***
Speed levels and unbalances	Rotational Speed 0...1500 rpm	Amplitude of rotor displacement	Increasing amplitudes, rotor circulates on a small orbit
Static loads	Load 850 N constant (step) Speed 0; 1500 rpm	Amplitude of rotor displacement	Small amplitude of rotor displacement Good accordance with results of simulation
	Load 850 N rising (ramp) Speed 0; 1500 rpm	Amplitude of rotor displacement	
Dynamic loads	Load 850 N sinusoidal, frequency up to 60 Hz Speed 0; 1500 rpm	Ratio of disturbed to undisturbed amplitude of rotor displacement	Amplitude of rotor displacement increases in range of resonance frequencies Damping is sufficient Maximum rotor displacement much smaller than the allowable rotor displacement Good accordance with results of simulation

The validation of the simulation tool MLDyn shows a very good accordance between measured results from experiment and calculated results from simulation.
Overall the experimental validation proves that the AMB's are applicable for the suspension of the GT-MHR.

4 Validation of diagnostics algorithms
4.1Introduction

In [4] a concept for the diagnostics of AMB machinery was developed. With the help of the FLP500 a validation of the diagnostics concept has been carried out. Main objective was the examination of the machine behaviour in normal operating state, different operating conditions and with the occurring of defined faults. The validation of the algorithms for the identification of faults in sensors, actuators and controllers was described in [4]. The validation was done by simulation models of the FLP500 because the creating of this faults at the real machine is not possible or to risky. The used simulation models have been validated in chapter 3. The behaviour in different operational conditions and the detection of radial forces (external forces) and unbalances (internal forces) are investigated at the real machine and described in this chapter. The used signals, features and the diagnostic concept are explained in [4]. For the diagnostics at the FLP500 the diagnostic system MLDia has been developed. The operation of this PC-based system especially for the monitoring of limit values and gradients to create alarm information and to trigger special data recording operations was also tested.

4.2 Results of the performed experiments
4.2.1 Reference values and speed dependence of the features

In order to detect deviations from the normal state the magnitudes of the signals and features in reference operation state and the dependence of this feature from the rotor speed have been analysed at the FLP500.
Fig 4.1 shows results over a speed range from 240 to 3180 rpm. The FLP500 was in this case operated without the load device. The rms values show an increase of the magnitudes to an maximum of 12 µm (shaft displacement in Fig. 4.1) respectively 900 mV (controller output in Fig. 4.2) at a critical rotor speed of 2200 rpm. Regarding the disturbance signals of about +-5 µm respectively +- 100 mV and the existing remaining unbalances of the rotor this speed dependencies are not significant.

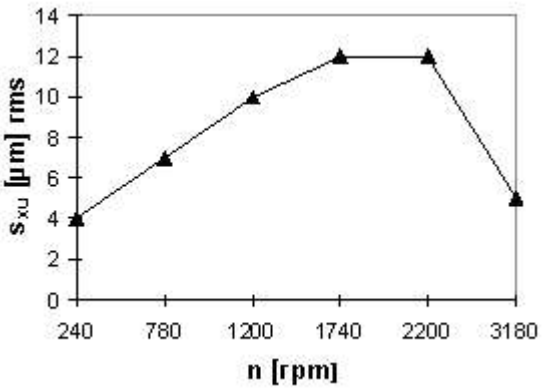

Fig. 4.1: Shaft displacement s_{xu}, (rms) by varying of n

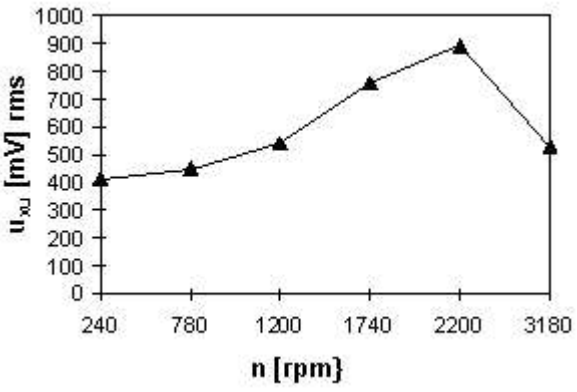

Fig. 4.2: Controller output u_{xu} (rms) by varying of n

Results with the load device in the speed range 0 – 1500 rpm shows Annex 1 as part of subsection 3.2.1.

4.2.2 Identification of internal and external loads

Influence of radial disturbance forces

The influence of static radial forces on the extracted features is shown in Figure 4.3. The radial force is acting in *y*-direction beginning from *t* = 1.6 s.

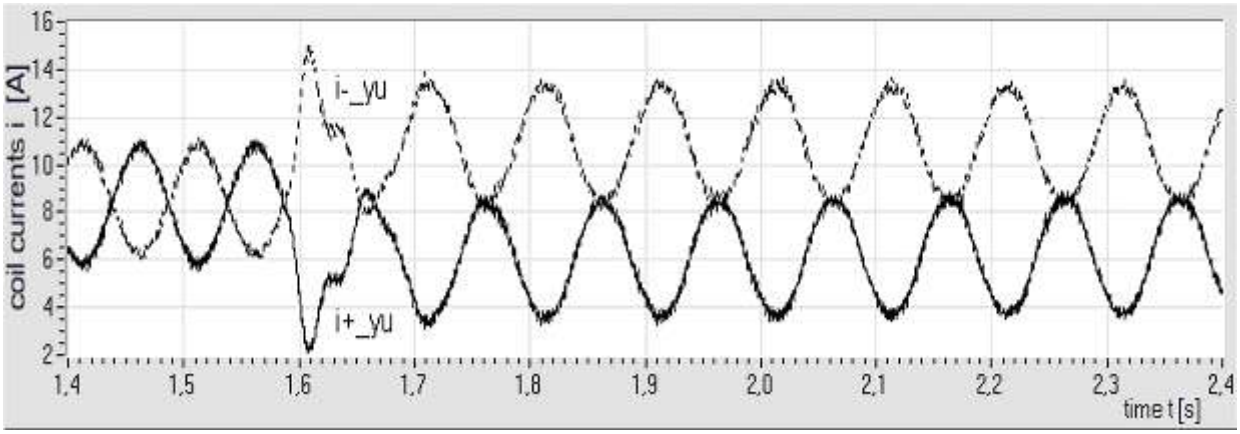

Fig. 4.3: Coil currents i_{+yu} and i_{-yu} with the radial force acting at *t* = 1.6 s

Characteristic features are the calculated mean values of the coil currents $\overline{i_{+yu}}$ and $\overline{i_{-yu}}$ and the calculated vectors of the actuating forces.

$\widetilde{s_{yu}}$: before fault = 15,1 µm, with fault = 12,8 µm

$\overline{i_{+yu}}$: before fault = 8,307 A, with fault = 6,669 A

$\overline{i_{-yu}}$: before fault = 8,505 A, with fault = 10,249 A

$\overline{i_{s,yu}}$: before fault = -0,1 A, with fault = -1,79 A

The radial force in each axis can be calculated from the mean values of current and displacement. With the force distribution in the axis and levels the radial force is locatable.

Influence of rotor unbalances

The Fig. 4.4b and 4.5b show the influence of rotor unbalances on the shaft displacement and the coil current.

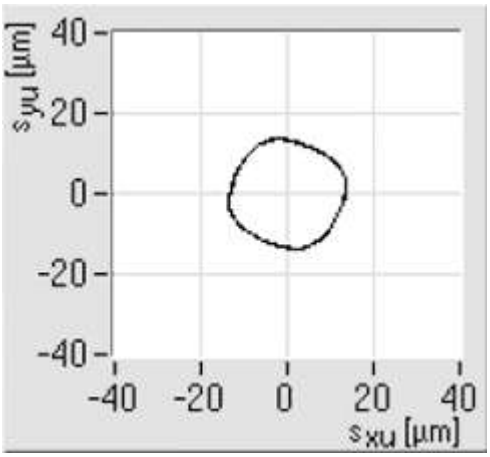

a) reference

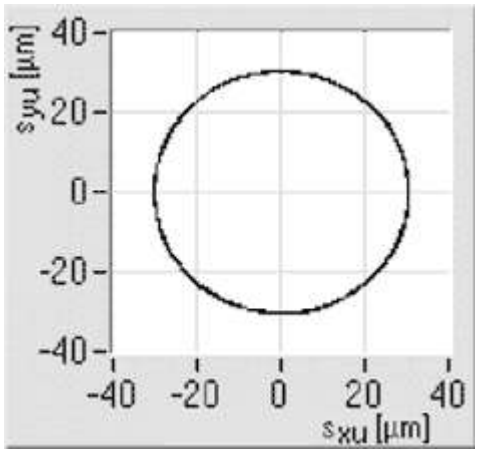

b) with unbalance acting

Fig 4.4: shaft displacement orbit s_{yu} vs. S_{xu}

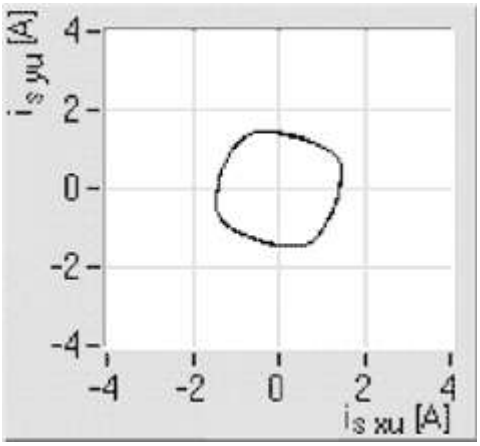

a) reference

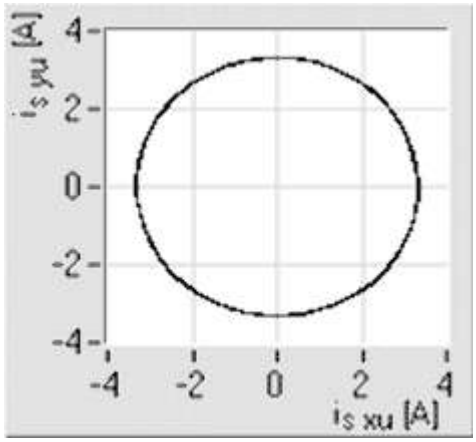

b) with unbalance acting

Fig 4.5: coil current orbit i_{s_yu} vs. i_{s_xu}

At a rotor speed of 876 rpm (ω = 92 s^{-1}) a force caused by eccentricities of the rotor and by the drive is acting in the reference state. With the additional unbalance caused by internal forces a disturbance force of 846 N is added: The rms value of the shaft displacement increases from 9,5 µm to 21,5 µm, the rms value of the coil current increases from 1,01 A to 2,33 A. The calculated rotating force increases and consists of the unbalance force and an additional force caused by the increased orbit of the shaft displacement .
The unbalance can be localized by using the ratios of the disturbance forces in the different levels of the radial bearings and the phase angles of the unbalance force vector.

Influence of the electric drive (motor)

Fig. 4.6 and Fig 4.7 show the influence of the electric drive (motor) on the orbits of the shaft displacement. The additional rotating force of the motor increases the orbit. The rotating speed is detectable as a characteristic frequency in the amplitude spectrum (Fig 4.8 and 4.9).

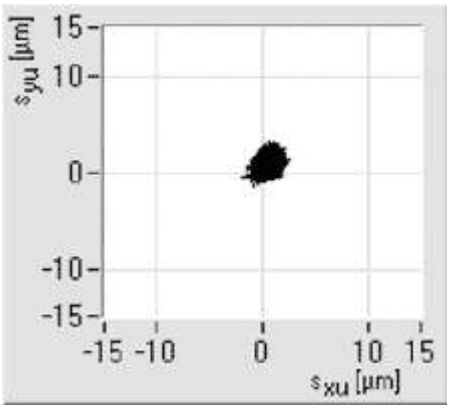

Fig. 4.6: Shaft displacement orbit s_{yu} vs. s_{xu} at 780 rpm, motor off

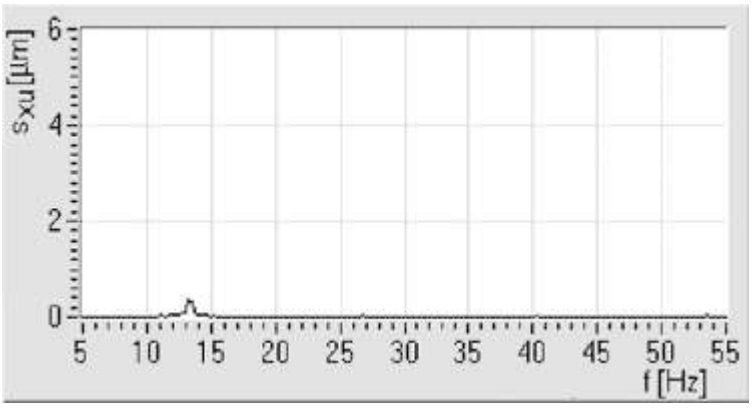

Fig. 4.7: Amplitude spectrum of the shaft displacement s_{xu} at 780 rpm, motor off

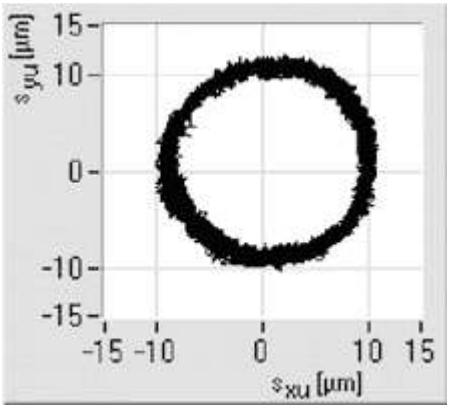

Fig 4.8: Shaft displacement orbit s_{yu} vs. s_{xu} at 780 rpm, motor on

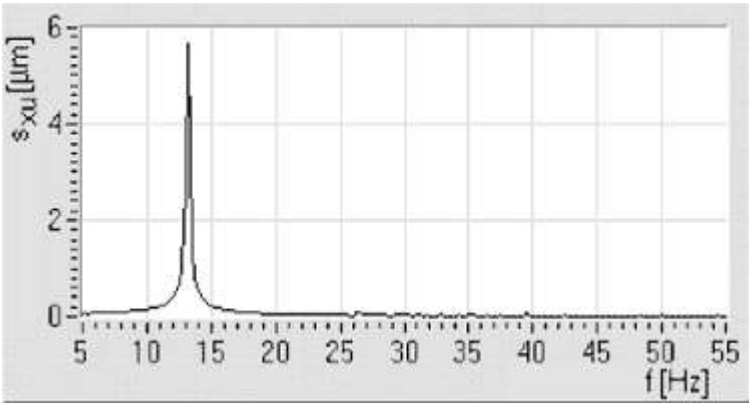

Fig. 4.9: Amplitude spectrum of the shaft displacement s_{xu} at 780 rpm, motor on

Rotating of the rotor shaft in the catcher bearings

If the AMB is switched off and the rotor shaft rotates in the catcher bearing it is possible to detect faults and wear of the catcher bearings. Fig. 4.10 and 4.11 depict the shaft displacement orbits and the amplitude spectrum of the shaft displacement for this case. Information on the condition of the catcher bearing can be received out of the deformation of the orbits and the characteristic frequencies.

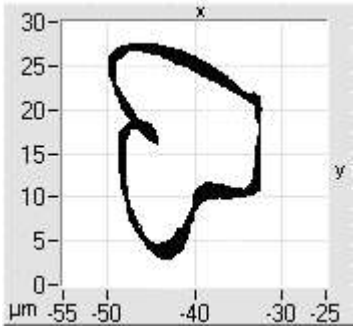

Fig. 4.10: Shaft displacement orbit s_{yu} vs. s_{xu} at 780 rpm, AMB and motor off

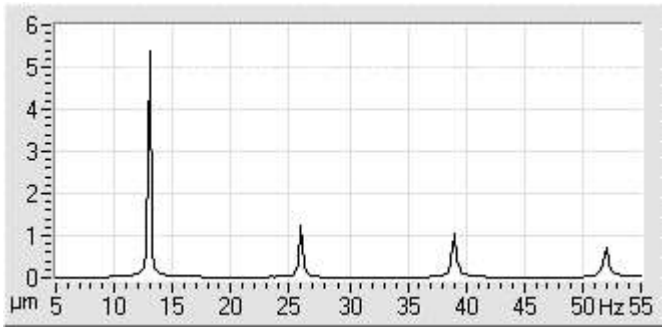

Fig. 4.11: Amplitude spectrum of the shaft displacement s_{xu} at 780 rpm, AMB and motor off

Significant frequencies of conventional roller bearings [5] are:

- the bearing cage rotation frequency whose magnitude increases with cage faults

$$f_C = \frac{1}{2} f_n \cdot \left(1 - \frac{DW}{DT} \cdot \cos\alpha\right) \tag{4.1}$$

- the roll over frequency of the outer bearing ring whose magnitude increases with defects of the outer bearing ring

$$f_O = \frac{1}{2} f_n \cdot z \cdot \left(1 - \frac{DW}{DT} \cdot \cos\alpha\right) \tag{4.2}$$

- roll over frequency of the inner bearing ring whose magnitude increases with defects of the inner bearing ring

$$f_I = \frac{1}{2} f_n \cdot z \cdot \left(1 + \frac{DW}{DT} \cdot \cos\alpha\right) \tag{4.3}$$

- rolling elements rotation frequency whose magnitude increases with defects of the rolling elements

$$f_R = \frac{1}{2} f_n \cdot \frac{DW}{DT} \cdot \left(1 - \frac{DW}{DT} \cdot (\cos\alpha)^2\right) \tag{4.4}$$

with: *z:* number of rolling elements
DW: diameter of the bearing
DT: rotating circle diameter
f_n: relative rotation between inner and outer ring
α: bearing specific constant

4.3 Validation of the diagnostic models
4.3.1 „Radial force“

A hierarchical structure in the shape of fault trees was designed and auxiliary linguistic variables were introduced for the diagnoses of radial forces. In this hierarchical structure fuzzy logic modules (FLM) were cascaded (Figure 4.12). The FLM realize the inference processing of the individual rule sets. The inputs of the FLM are linguistic input variables which are fuzzified by the FLM or the results of sub-rules. The Operator for the fuzzy AND is the algebraic product and for the accumulation of the individual conclusions the maximum operator. The defined linguistic variables and sets are given in Fig 4.13 – 4.16 and Table 4.2.

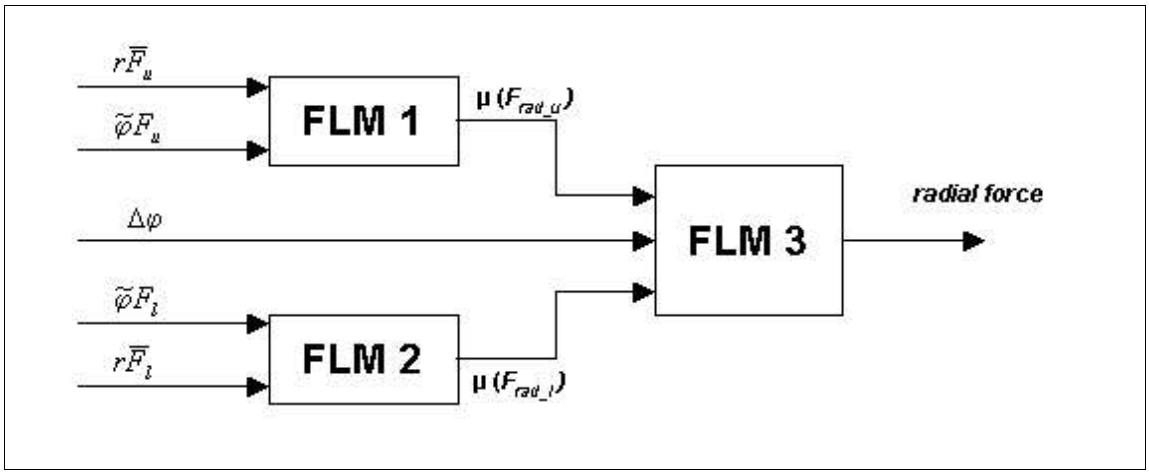

Fig. 4.12: Cascaded fuzzy logic modules (FLM) for the diagnostics *radial force*

The inputs for FLM 1 and FLM 2 are the mean values $r\overline{F}$ of the force vector magnitudes of the upper and lower radial magnetic bearing and the rms values $\tilde{\varphi}F$ of the force vector angles. FLM 1 and FLM 2 calculate the auxiliary variables F_{rad_u} and F_{rad_l} with the individual rules

IF $\tilde{\varphi}F_u$ = *K* AND $r\overline{F_u}$ = *G* THAN F_{rad_u}:= *G*

IF $\tilde{\varphi}F_l$ = *K* AND $r\overline{F_l}$ = *G* THAN F_{rad_l}:= *G*

F_{rad_u} and F_{rad_l} are used by FLM 3 together with the phase difference $\Delta\varphi$ between the force vectors angles from the upper and lower bearing.

FLM 3 calculates the diagnostics *radial force* using the basic rule

IF F_{rad_u} AND F_{rad_l} AND $\Delta\varphi$ THAN *radial force*

and the rule base shown in Table 4.1.

Table 4.1: Rule base of FLM 3

radial force				$\Delta\varphi$		
				0	**180**	**1**
F_{rad_l}	**K**	F_{rad_u}	**K**	**X**	**X**	**X**
	K		**G**	**X**	**X**	**Frub**
	G		**K**	**X**	**X**	**Frlb**
	G		**G**	**Frbb**	**Frob**	**X**

Table 4.2: Linguistic variables for the diagnostics *radial force*

linguistic variable	value	remark
F_{rad_u}, F_{rad_l}, $r\overline{F_u}$, $r\overline{F_l}$, $\tilde{\varphi}F_u$, $\tilde{\varphi}F_l$	G	Big (Groß)
	K	Small (Klein)
$\Delta\varphi$	0	0°
	180	180°
	1	(don‘t care)
radial force	Frub	radial force in the upper bearing level
	Frlb	radial force in the lower bearing level
	Frbb	radial force between the upper and lower bearing level
	Frob	radial force below the lower or over the upper bearing level

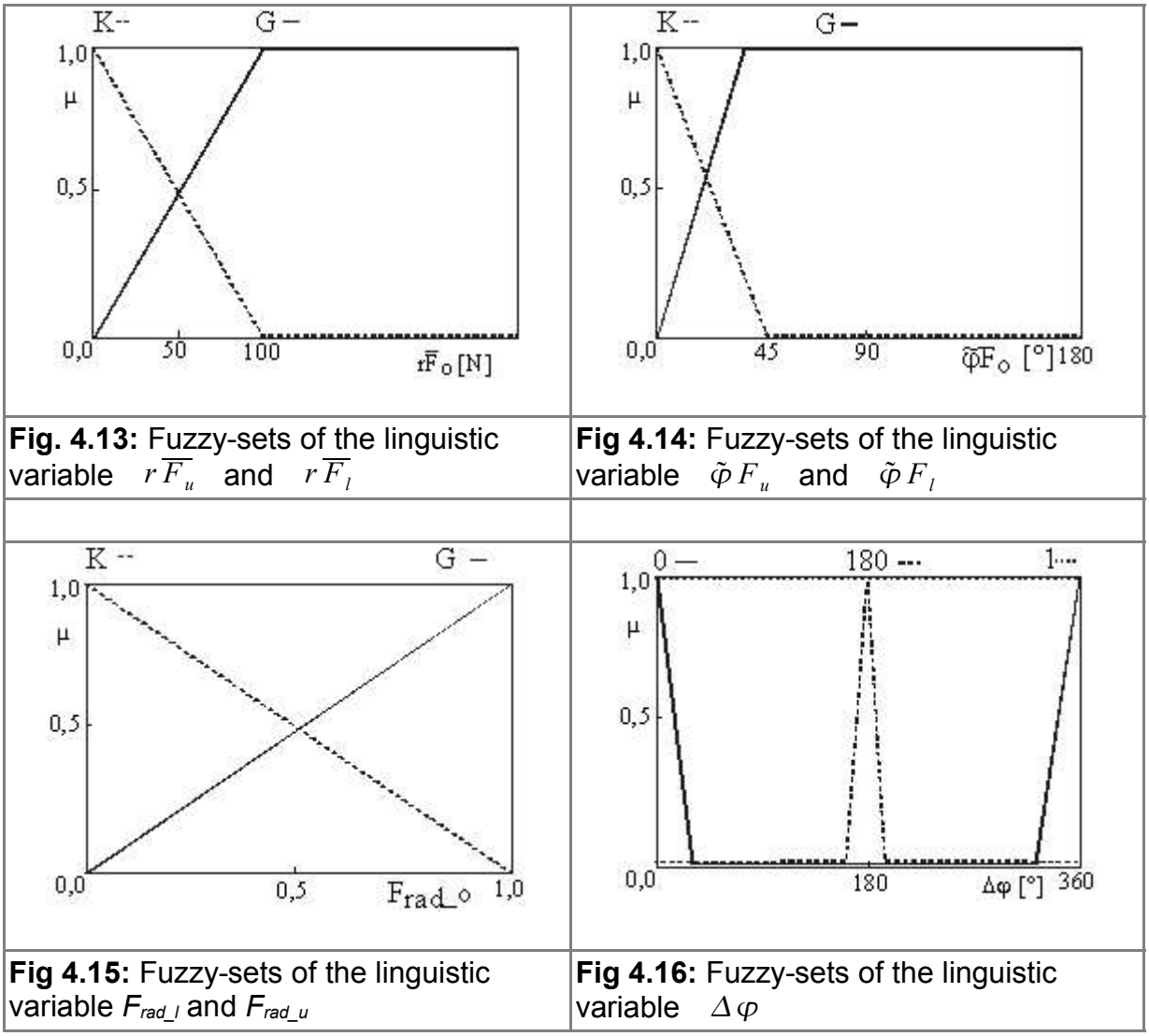

Fig. 4.13: Fuzzy-sets of the linguistic variable $r\overline{F_u}$ and $r\overline{F_l}$

Fig 4.14: Fuzzy-sets of the linguistic variable $\tilde{\varphi}F_u$ and $\tilde{\varphi}F_l$

Fig 4.15: Fuzzy-sets of the linguistic variable F_{rad_l} and F_{rad_u}

Fig 4.16: Fuzzy-sets of the linguistic variable $\Delta\varphi$

The output of FLM 3 is the diagnostics *radial force* with the fulfilment degrees of the sets of the fault classes:

- *Frub*: radial force in the upper bearing level
- *Frlb*: radial force in the lower bearing level
- *Frbb*: radial force between the upper and lower bearing level
- *Frob*: radial force below the lower or over the upper bearing level

Figure 4.17a shows diagnostics results with simulated radial forces. The force acted below the lower bearing starting from t = 1.5 s. The degree of fulfilment of the corresponding fault class *Frob* fired correctly with the value of 0.98, the other degrees remained below 0.1. Results of analogous experiments on the test facility FLP500 are shown in Fig. 4.17b. The fault was also correctly identified with a degree of fulfilment of 0.7.

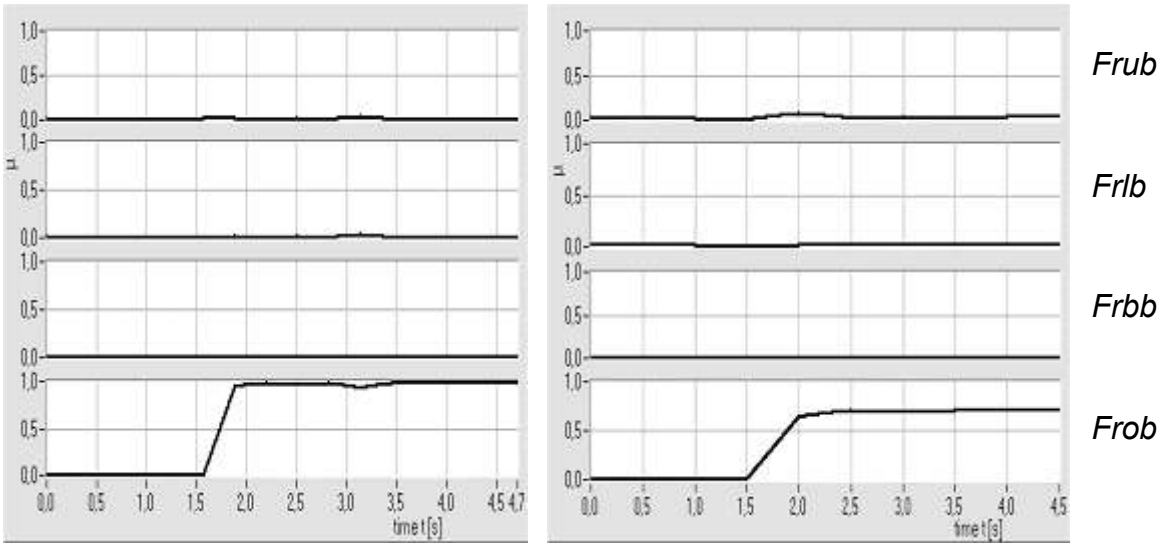

a) Simulation with *MLDyn* b) Experiment on the FLP500

Fig. 4.17: Degrees of fulfilment of the fault classes with the occurrence of the fault "radial force below the lower magnetic bearing"

4.3.2 „Unbalances“

Unbalances are detectable with increases of the rms values $r\tilde{F}$ of the force vector magnitudes at a constant angle of the rotor. With a trigger-point at a rotor angle of $\gamma = 0°$ (key-phasor) the angles γ_{Fmax} at the force vector maxima are measured. For the detection of the constant angle the linguistic variable $\tilde{\gamma}$ is calculated as the rms value of γ_{Fmax} over a series of rotor revolvings. The increase of the forces caused by critical rotor speeds is considered by using the rotor speed as linguistic variable *n*.

For the diagnostics of unbalances fuzzy logic modules (FLM) were cascaded (Fig. 4.18). The Operator for the fuzzy AND is the algebraic product and for the accumulation of the individual conclusions the maximum operator. The defined linguistic variables and sets are given in Fig 4.19 – 4.21 and Table 4.3.

FLM 4 and FLM 5 calculate the variables F_{unb_u} and F_{unb_l} using the basic rules

IF $\tilde{\gamma}_u$ = *K* AND $r\tilde{F}_u$ = *G* AND *n* = *NK* THAN F_{unb_u}

IF $\tilde{\gamma}_l$ = *K* AND $r\tilde{F}_l$ = *G* AND *n* = *NK* THAN F_{unb_l}

Fig. 4.18: Cascaded fuzzy logic modules (FLM) for the diagnostics *unbalance*

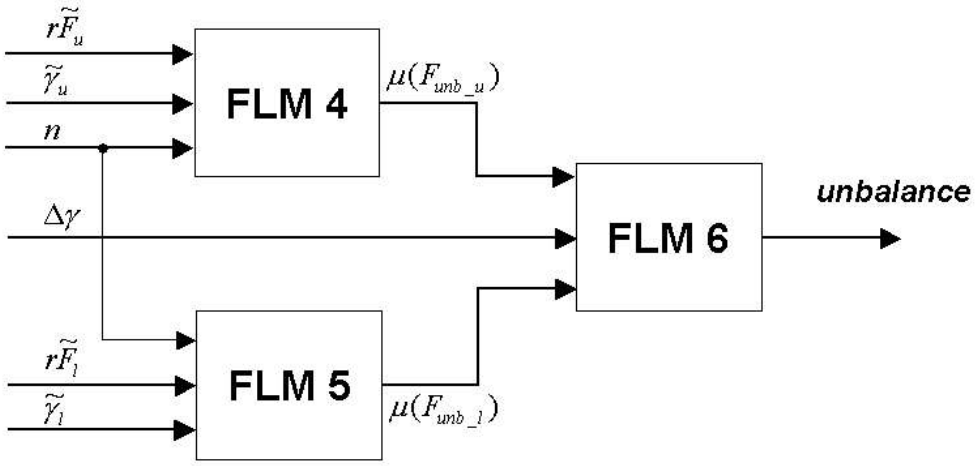

FLM 6 calculates the diagnostics *unbalance* with $\Delta\gamma$ and the outputs of FLM 4 and FLM using the basic rule

IF F_{unb_u} AND F_{unb_l} AND $\Delta\gamma$ THAN *unbalance*

and the rule base shown in Table 4.3.

$\Delta\gamma$ is calculated by

$\Delta\gamma = |\gamma_{Fmax,u} - \gamma_{Fmax,l}|$

$\gamma_{Fmax,u}$ ...angle of the unbalance vector of the upper bearing level

$\gamma_{Fmax,l}$ ...angle of the unbalance vector of the lower bearing level

Table 4.3: Rule base of FLM 6

unbalance				$\Delta\gamma$			
				0	**180**	**W**	**1**
F_{unb_l}	**K**	F_{unb_u}	**K**	**X**	**X**	**X**	**X**
	K		**G**	**X**	**X**	**X**	**Uub**
	G		**K**	**X**	**X**	**X**	**Uob**
	G		**G**	**Ubl**	**Uob**	**Uw**	**X**

Table 4.4: Linguistic variables for the diagnoses *unbalance*

linguistic variable	value	remark
F_{unb_u}; F_{unb_l} $r\tilde{F}_u$, $r\tilde{F}_l$, $\tilde{y}_u$, $\tilde{y}_l$	G	Big (Groß)
	K	Small (Klein)
n	NK	Not Critical
	KR	Critical
$\Delta\gamma$	0	0°
	180	180°
	W	warped
	1	(don't care)
unbalance	Uub	unbalance in the upper bearing level
	Ulb	unbalance in the lower bearing level
	Ubb	unbalance between the upper and lower bearing level
	Uob	Unbalance below the lower or over the upper bearing level
	Uw	Unbalance warped

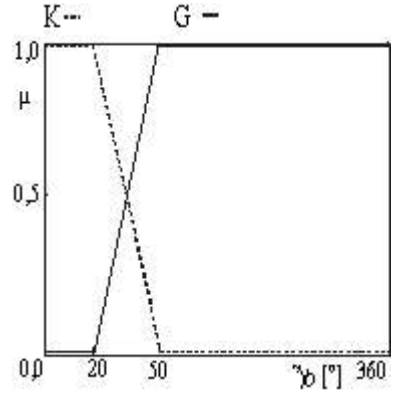

Fig. 4.19: Fuzzy-sets of the linguistic variable $\tilde{y}_u$ and $\tilde{y}_l$

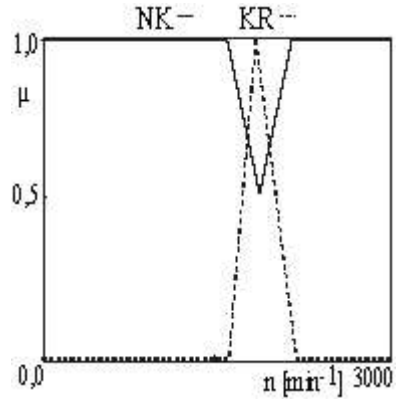

Fig. 4.20: Fuzzy-sets of the linguistic variable *n*

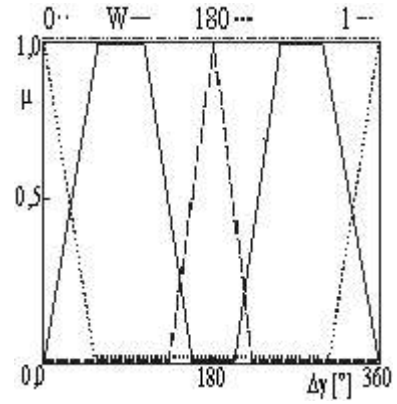

Fig. 4.21: Fuzzy-sets of the linguistic variable $\Delta\gamma$

The output of FLM 6 is the diagnostics *unbalance* with the fulfilment degrees of the sets of the fault classes:

- *Uub*: unbalance in the upper bearing level
- *Ulb:* unbalance in the lower bearing level
- *Ubb*: unbalance between the upper and lower bearing level
- *Uob*: unbalance below the lower or over the upper bearing level
- *Uw:* unbalance warp (multiple unbalances at different positions)

Fig. 4.22 shows the diagnostics result if only residual unbalances caused by eccentricities of the rotor and by the drive are acting between the bearings. The correct diagnostics result *Ubb* fires with a fulfilment of 0,96. If a additional unbalance of 0,1 kgm is added at the lower end of the shaft with a phase difference of 60° to the residual unbalance the diagnostics result is the diagnostics *Uw* with a fulfilment of 0,8 (Fig. 4.23). That is caused because 2 different unbalances are acting. To identify the

added unbalance the input signals are adapted to the reference state by calculating the residue of the different states and using this values for the input of the FLM. Fig 4.24 shows the diagnostics result with the correct identified fault *Uob* = 0,94. This example shows that it is possibly to identify multiple faults.

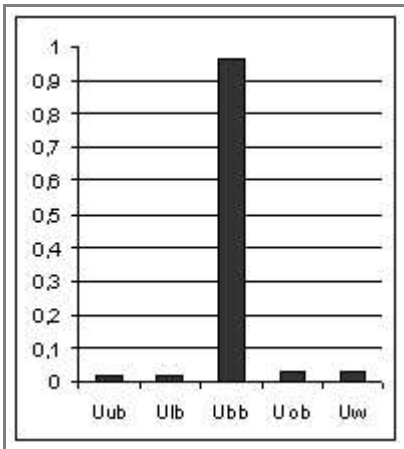

Fig. 4.22: diagnostics result at reference state with residual unbalance

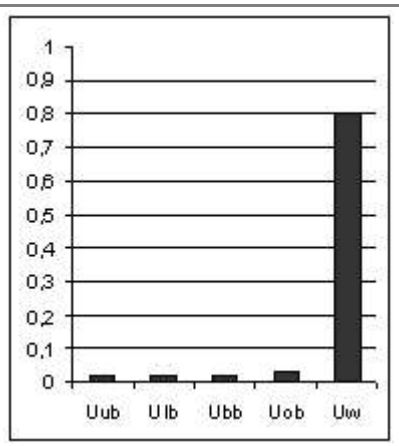

Fig. 4.23: diagnostics result with additional unbalance

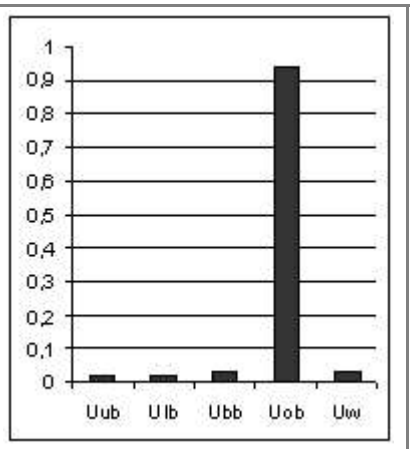

Fig. 4.24: diagnostics result with additional unbalance and calculation of the residue

Fig. 4.25 shows the correct diagnostics result if the residual unbalance is acting and an additional radial force according to experiment in 4.3.1. The additional radial doesn't interfere with the diagnostics of the unbalance. The correct unbalance *Ubb* is diagnosed with a fulfilment of 0,8. The wrong diagnostics *Uw* fires with a fulfilment of 0,2 which is negligible.

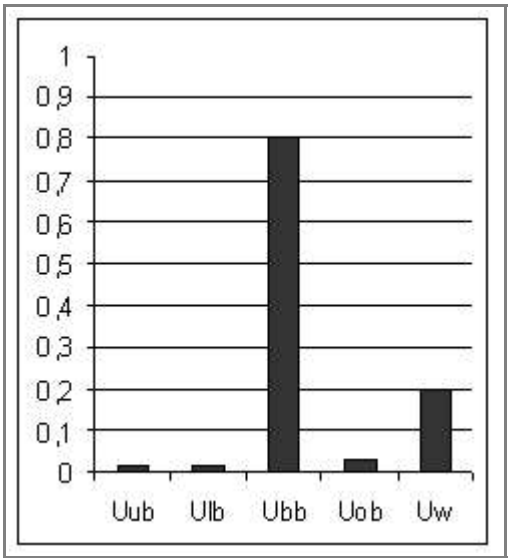

Fig. 4.25: diagnostics result with residual unbalance and radial force

4.4 Monitoring of limit values and gradients

The extracted magnitudes of the features are monitored on transgression of limits and trends. The transgression of a limit determines the occurrence of a fault and results in an alarm or data storage routine. The limit value checking gives a fast way to detect critical changes of the machine condition.

Table 4.5 shows the used features for the limit value checking and the causes for the transgression.

Table 4.5: Overview of the used features for the limit value monitoring

signal	feature	fault
shaft displacement	maximum/ minimum	transgression of the measurement range by defect of the sensor, cable circuit breaks or at critical speed
magnitude of the shaft displacement signal vector	maximum	danger of damage by rotor-stator contact
coil current	maximum	coil currents near the possible maximum current, non-linear behaviour
coil current	minimum	coil current to low, non-linear behaviour

The limit value checking has been realised with the PC-based diagnostic system MLDia. Main point of the validation was the speed of recognition. The limit values has been set at values which are exceeded at the critical rotor speed. The system showed a correct identification of all transgressions and the full storage of all data at the event.

4.5 Conclusion

In this document the concept of diagnostics for AMB using system inherent signals was validated. Knowledge-based models for the diagnostics using fuzzy logic have been successfully tested and verified. The defined fuzzy sets, operators and the selected rules realise a correct identification of occurring faults with a minimized effort of calculation. Using the concept of cascaded fuzzy logic modules the transparency of the whole systems was preserved even with a large number of features and rules. The developed diagnostic-system MLDia was able to calculate all diagnostics models, display and save the relevant information and carry out the limit value checking simultaneously.

Main aims of diagnostics are

- early detection of changes in the systems condition (faults)
- identification and localisation of faults
- proposing of approbiate counter measures

in order to increase the safety, reliability and lifespan of the magnetic suspended system and to decrease the costs for the maintenance.

References:

[1] OKBM; ISTC 1261 Technical Report

[2] Functional Requirements for GT-MHR: HTR-E-02/06-D-3-1-1

[3] Load Analysis – Real Time Investigations: HTR-E-03/10-D-3-1-2-2

[4] Concept Proposal for AMB and Diagnostic: HTR-E-04/02-D-3-2-1-2

[5] Sturm, A.: Wälzlagerdiagnose an Maschinen und Anlagen,
Verlag TÜV-Rheinland, 1986

Annex 1 – Speed levels and unbalances

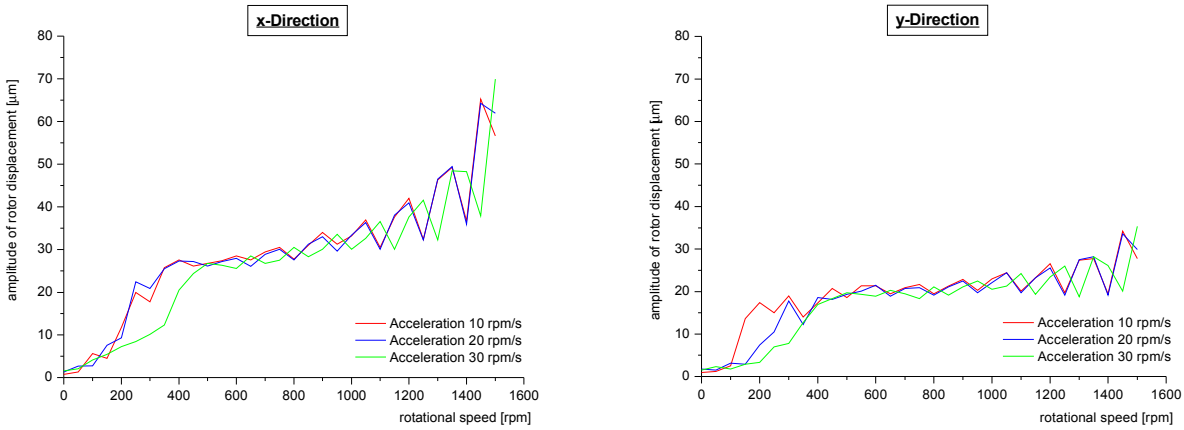

Amplitude of rotor displacement vs. Rotational speed for the upper radial AMB's

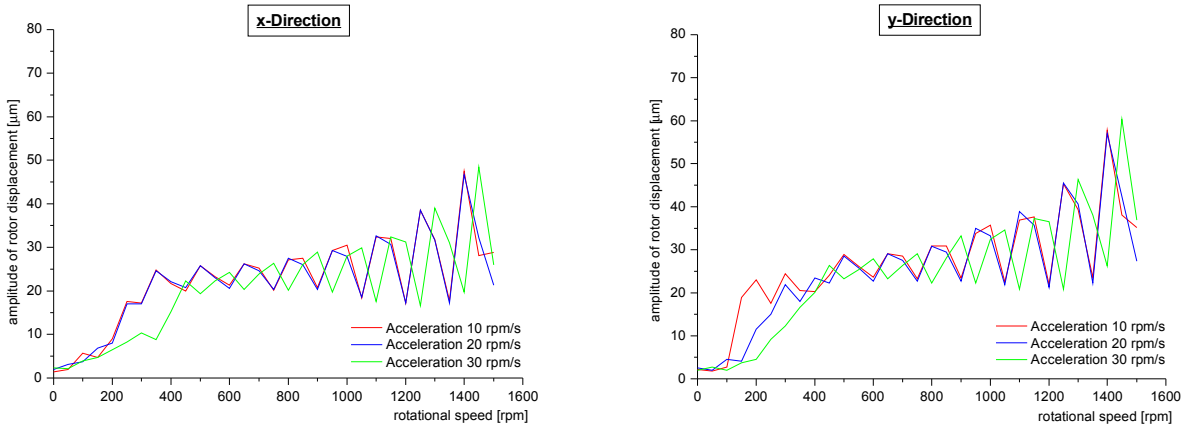

Amplitude of rotor displacement vs. Rotational speed for the lower radial AMB's

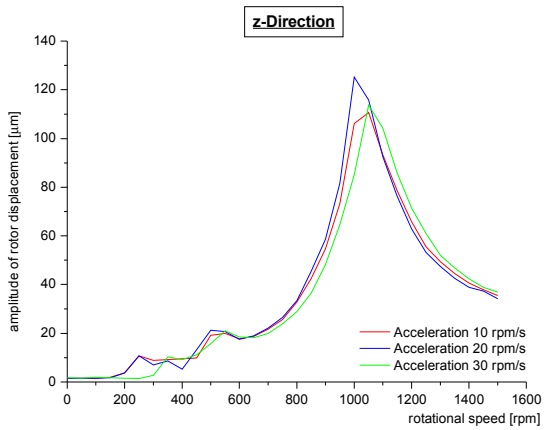

Amplitude of rotor displacement vs. Rotational speed for the axial AMB's

Annex 2 – Static Loads

Load introduction via step function at 0 rpm:

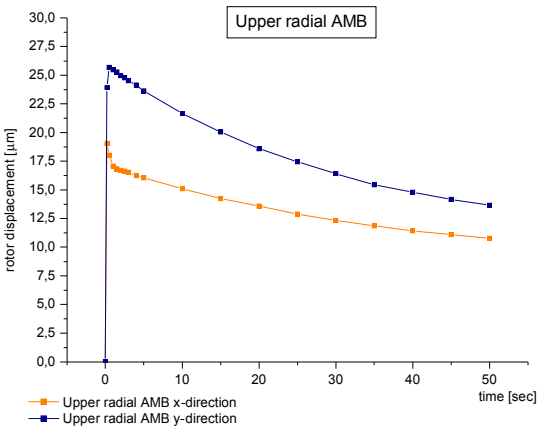

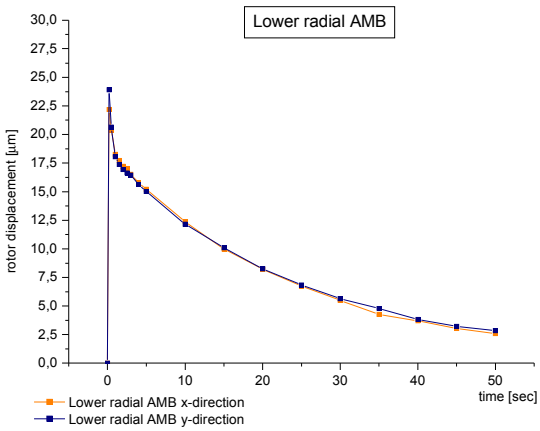

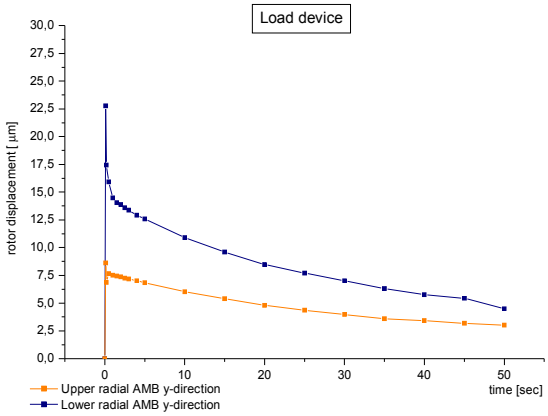

Rotor displacement vs. Time for the load introduction in the levels of upper and lower AMB's and load device.

Load introduction via step function at 1500 rpm:

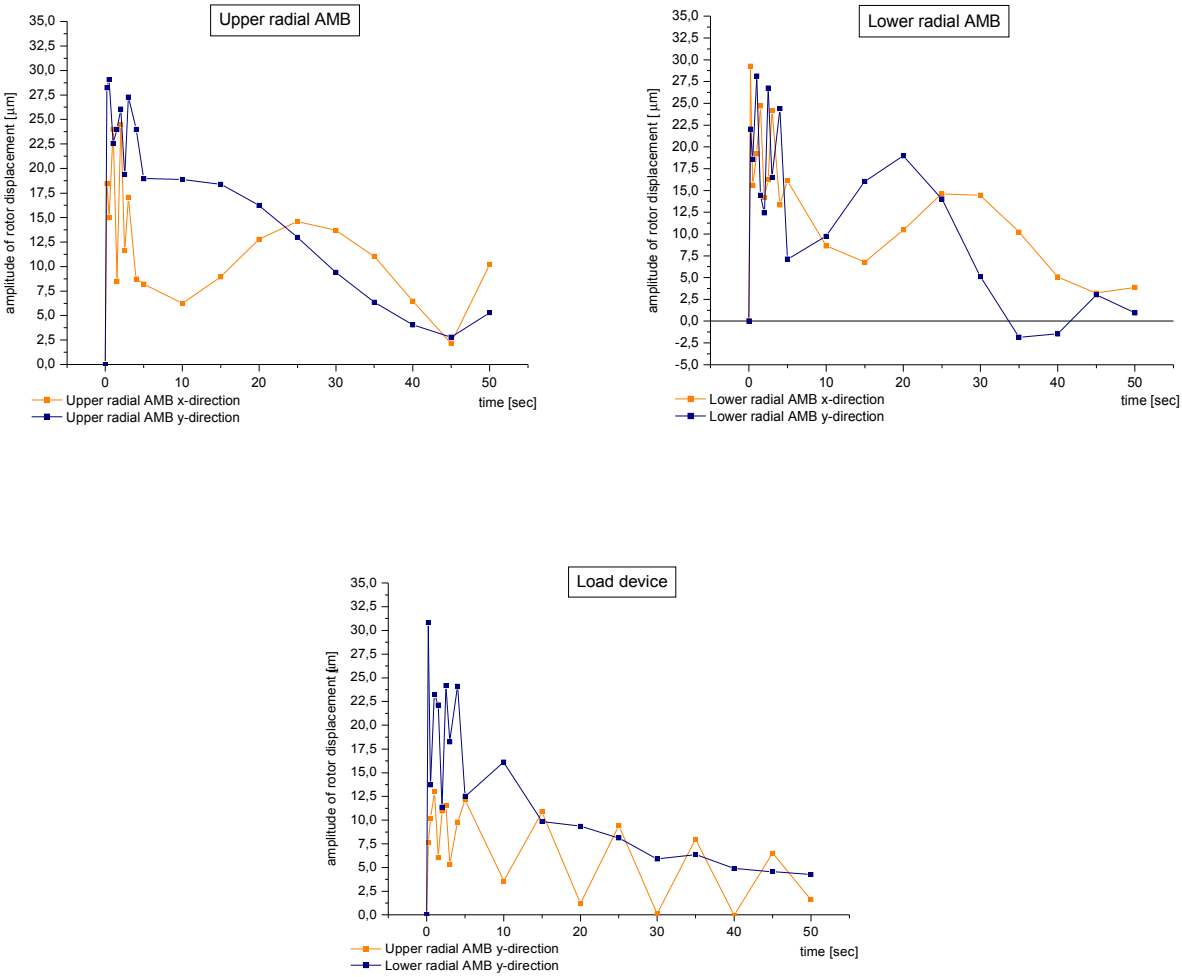

Amplitude of rotor displacement vs. Time for the load introduction in the levels of upper and lower AMB's and load device.

Load introduction via ramp function at 0 rpm:

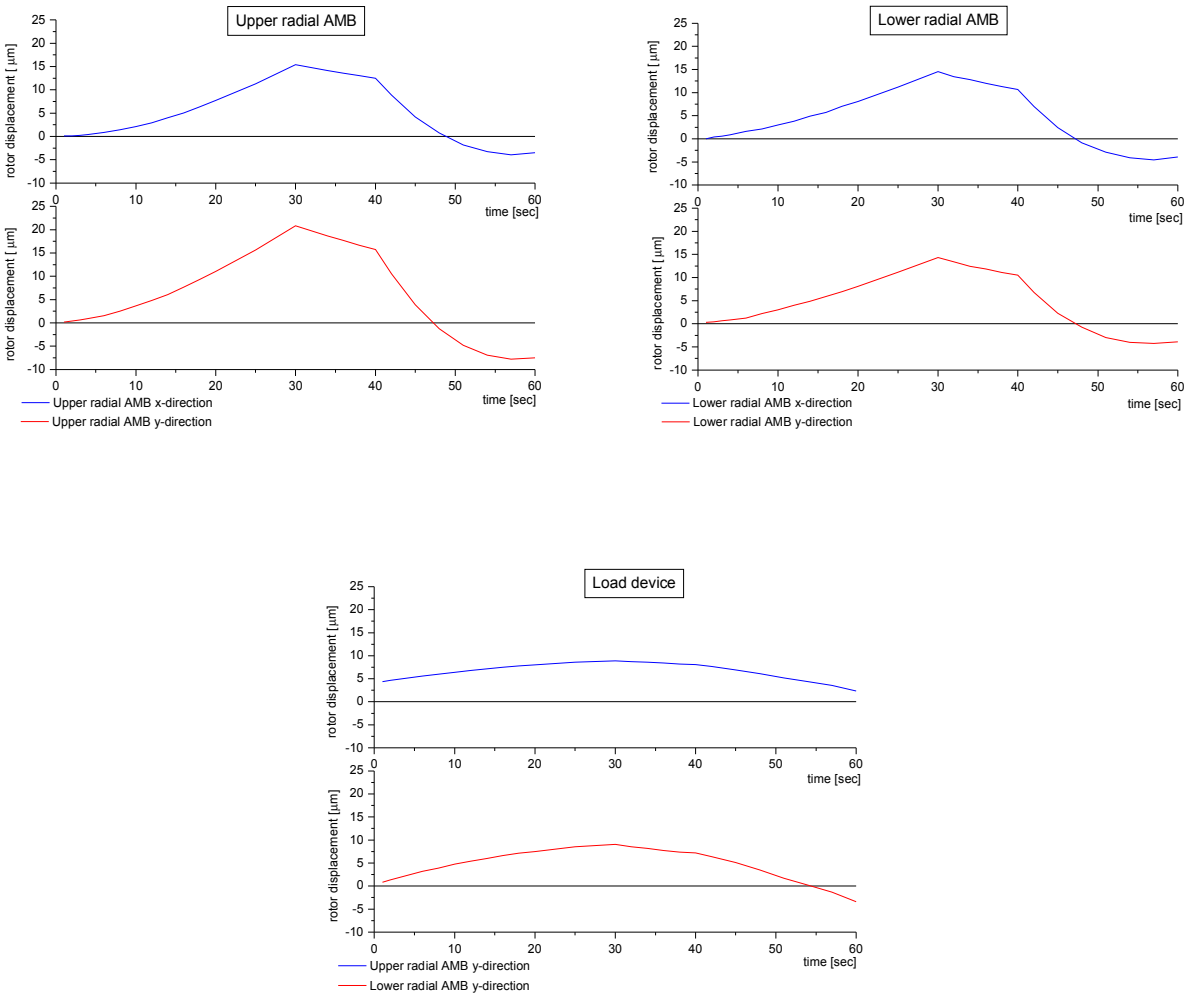

Rotor displacement vs. Time for the load introduction in the levels of upper and lower AMB's and load device.

Load introduction via ramp function at 1500 rpm:

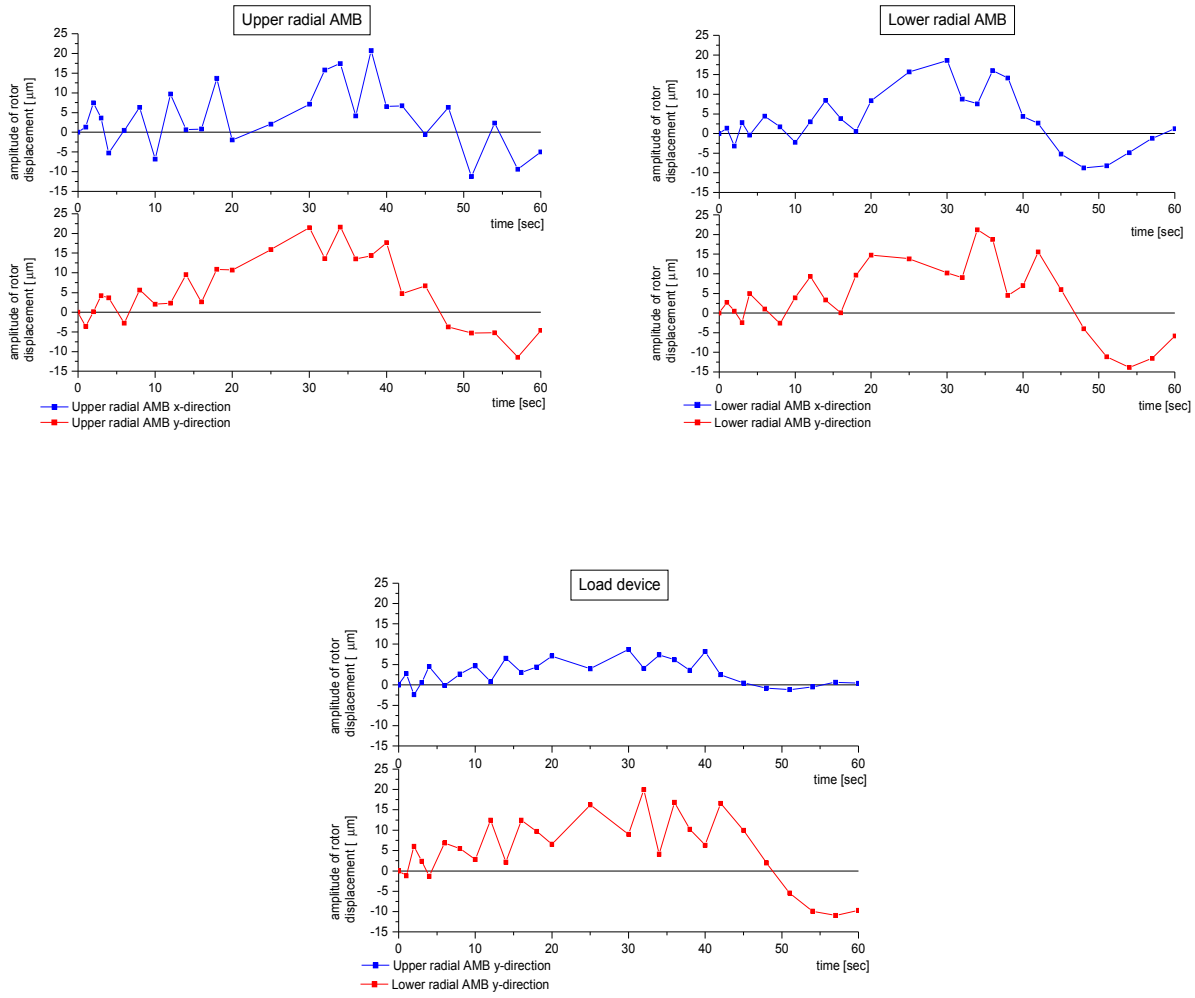

Amplitude of rotor displacement vs. Time for the load introduction in the levels of upper and lower AMB's and load device.

Annex 3 – Dynamic Loads

Load introduction via sinusoidal function at 0 rpm

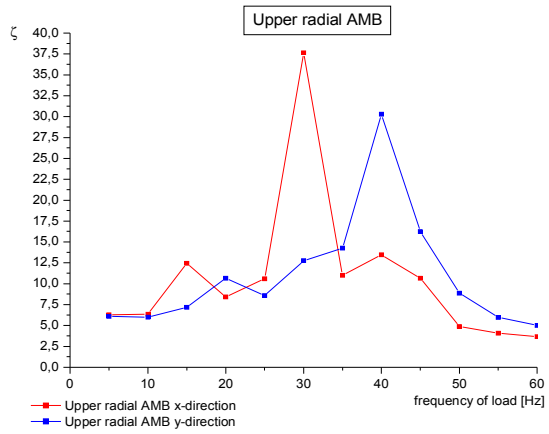

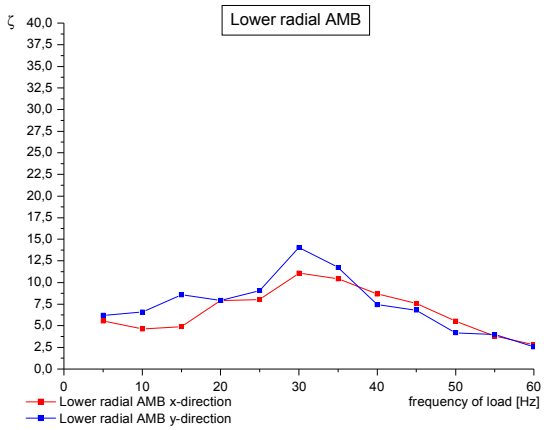

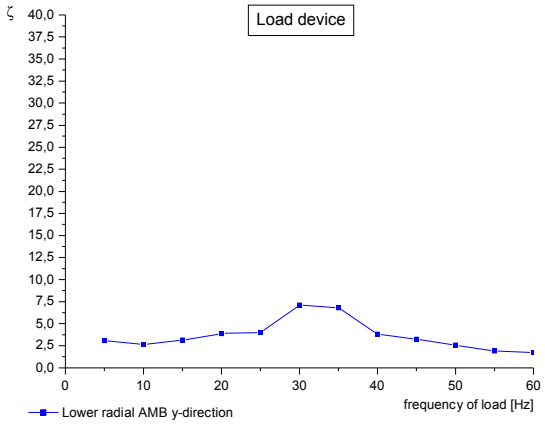

Ratio of disturbed to undisturbed amplitude of rotor displacement for the load introduction in the levels of upper and lower AMB's and load device.

Load introduction via sinusoidal function at 1500 rpm

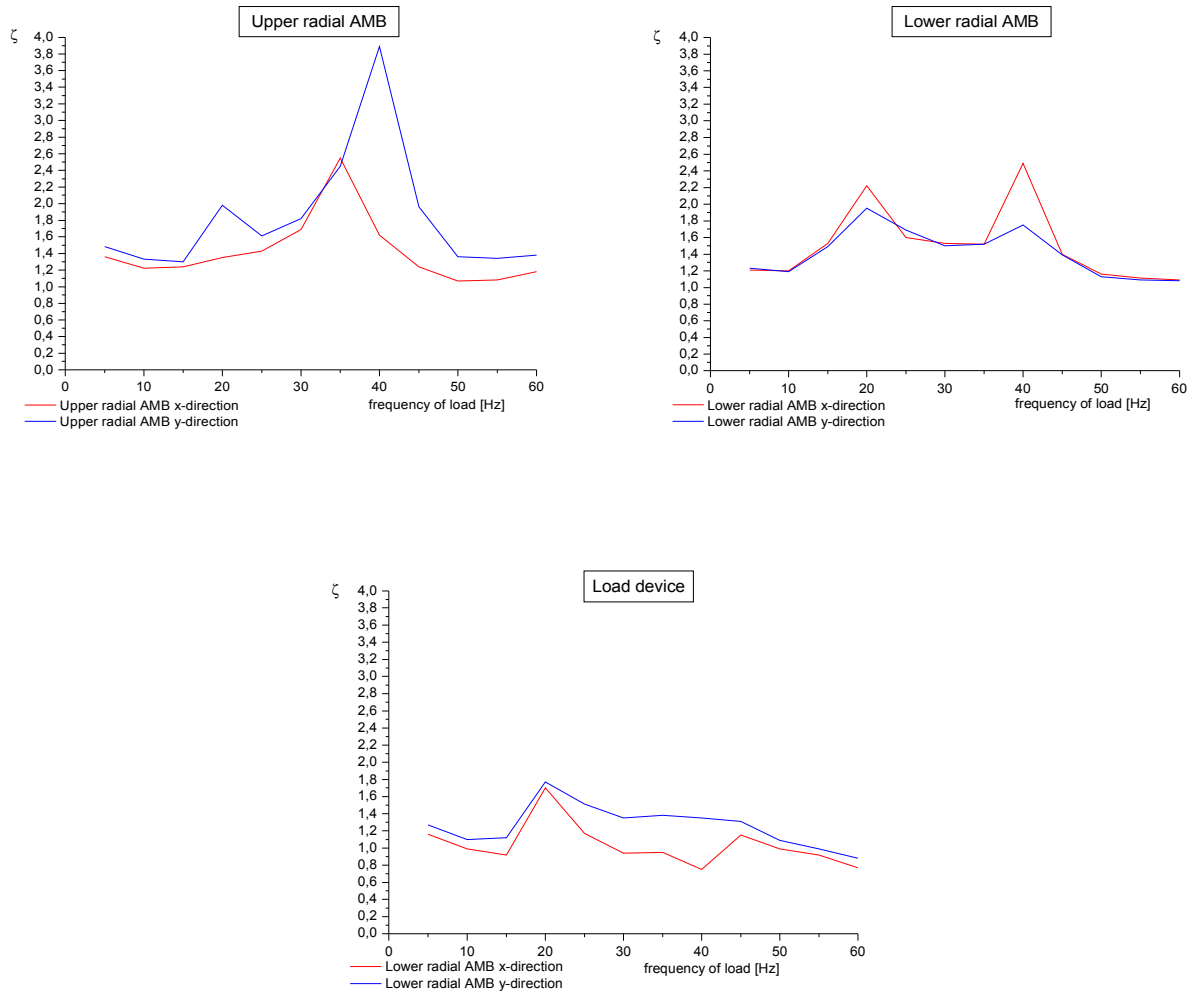

Ratio of disturbed to undisturbed amplitude of rotor displacement for the load introduction in the levels of upper and lower AMB's and load device.